nagra
National Cooperative for
the Disposal of Radioactive Waste

TECHNICAL REPORT 90-39

GRIMSEL TEST SITE

THE GRIMSEL MIGRATION EXPERIMENT: A HYDROGEOCHEMICAL EQUILIBRIUM TEST

J. EIKENBERG
B. BAEYENS
M.H. BRADBURY

PSI, Würenlingen and Villigen

MAY 1991

GRIMSEL TEST SITE / SWITZERLAND
A JOINT RESEARCH PROGRAM BY

- NAGRA – National Cooperative for the Storage of Radioactive Waste, Wettingen, Switzerland
- BGR – Federal Institute for Geoscience and Natural Resources, Hannover, Federal Republic of Germany
- GSF – Research Centre for Environmental Sciences, Munich, Federal Republic of Germany

Hardstrasse 73, CH-5430 Wettingen / Switzerland, Telephone + 42-56-37 11 11

nagra National Cooperative for the Disposal of Radioactive Waste

TECHNICAL REPORT 90-39

GRIMSEL TEST SITE

THE GRIMSEL MIGRATION EXPERIMENT: A HYDROGEOCHEMICAL EQUILIBRIUM TEST

J. EIKENBERG
B. BAEYENS
M.H. BRADBURY

PSI, Würenlingen and Villigen

MAY 1991

GRIMSEL TEST SITE / SWITZERLAND
A JOINT RESEARCH PROGRAM BY

- NAGRA – National Cooperative for the Storage of Radioactive Waste, Wettingen, Switzerland
- BGR – Federal Institute for Geoscience and Natural Resources, Hannover, Federal Republic of Germany
- GSF – Research Centre for Environmental Sciences, Munich, Federal Republic of Germany

Hardstrasse 73, CH-5430 Wettingen / Switzerland, Telephone + 42-56-37 11 11

FOREWORD

Concepts for the disposal of radioactive waste in geological formations lay great weight on acquiring extensive knowledge of the proposed host rock and the surrounding rock strata. For this reason, Nagra has, since May 1984, been operating the **Grimsel Test Site (GTS)** which is located at a depth of 450 m in the crystalline rock of the Aare Massif of the Central Swiss Alps. The general objectives of the research being carried out in this underground laboratory include

- the build-up of know-how in planning, performing and interpreting field experiments in various scientific and technical disciplines.

- the acquisition of practical experience in the development of investigation methodologies, measuring techniques and test equipment which will be of use during actual repository site explorations.

The GTS is operated by Nagra and, on the basis of a German-Swiss co-operative agreement, various experiments are carried out by Nagra, the Federal Institute for Geoscience and Natural Resources (Bundesanstalt für Geowissenschaften und Rohstoffe, BGR) and the Research Center for Environmental Sciences (Forschungszentrum für Umwelt und Gesundheit GSF). The Grimsel projects of both GSF and BGR are supported by the German Federal Ministry for Research and Technology (BMFT). NTB 85-46 (English version) and NTB 85-47 (German version) provide an overview of the German-Swiss investigation programme. In a special issue of the Nagra Bulletin 1988 (English version) and in Nagra Informiert 1+2/1988 (German version) the status of the programme up to 1988 is described.

Within this framework, the **Radionuclide Migration Experiment (MI)** has been an extensive contribution from Nagra to the Grimsel programme. MI is a multidisciplinary study aimed at investigating solute transport in fractured media. Field work is complemented by a programme of hydrodynamic, chemical and transport modelling, along with supporting laboratory studies. This project, initiated in 1985 and currently planned to be terminated in 1993, was initially conceived as a collaborative project between Nagra and the Paul Scherrer Institute (PSI). Since 1987, radiotracer field tests have also been carried out with the Institute of Hydrology of GSF Munich-Neuherberg. In 1989 a bilateral collaboration agreement was signed with the Japanese Power Reactor and Nuclear Fuel Development Corporation (PNC) and the support under this co-operation resulted in a substantial extension of the Grimsel Radionuclide Migration project.

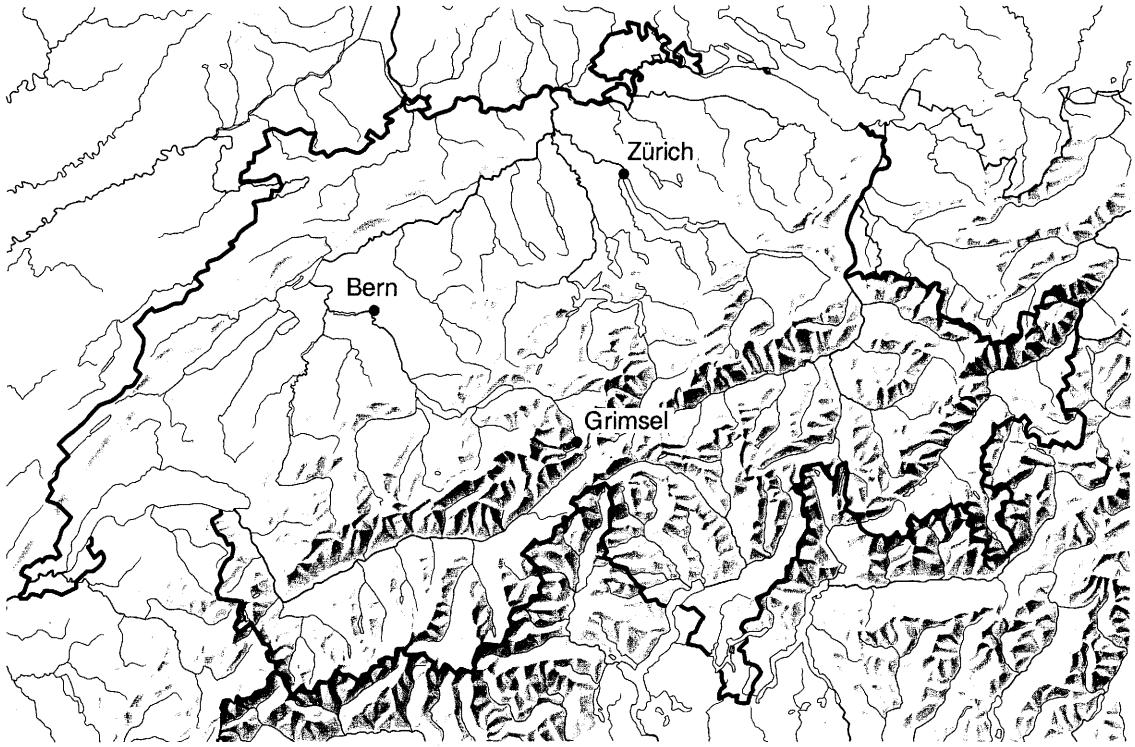

Location of Nagra's underground test facility at the Grimsel Pass in the Central Alps (Bernese Alps) of Switzerland (approximate scale 1 cm = 25 km).

Geographische Lage des Nagra Felslabors am Grimselpass (Berner Oberland) in den schweizerischen Zentralalpen (Massstab: 1 cm = ca. 25 km)

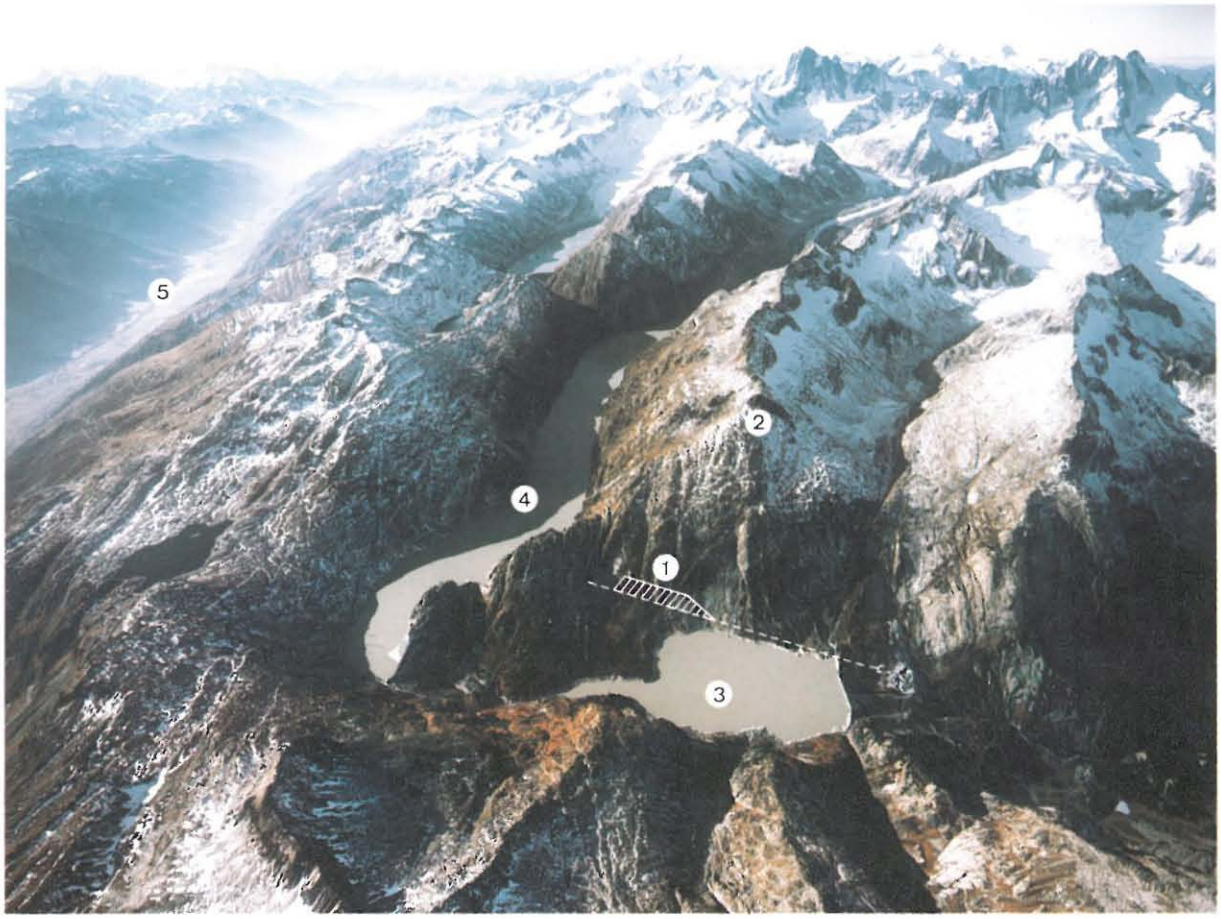

GRIMSEL-GEBIET

Blick nach Westen

1 Felslabor
2 Juchlistock
3 Räterichsbodensee
4 Grimselsee
5 Rhonetal

GRIMSEL AREA

View looking West

1 Test Site
2 Juchlistock
3 Lake Raeterichsboden
4 Lake Grimsel
5 Rhone Valley

FLG FELSLABOR GRIMSEL
GTS *GRIMSEL TEST SITE*

Situation

0 100 m

- Zugangsstollen/*Access tunnel*
- Fräsvortrieb/*by tunnel boring machine*
- Sprengvortrieb/*excavated by blasting*
- Zentraler Aaregranit ZAGR / *Central Aaregranite CAGR*
- Biotitreicher ZAGR / *CAGR with high content of biotite*
- Grimsel-Granodiorit / *Grimsel-Granodiorite*
- Scherzone/*Shear zone*
- Lamprophyr/*Lamprophyre*
- Wasserzutritt/*Water inflow*
- SB Sondierbohrung/*Exploratory borehole*
- US US Bohrung/*US borehole*

ZB	Zentraler Bereich/*Central facilities*
AU	Auflockerung/*Excavation effects*
BK	Bohrlochkranz/*Fracture system flow*
EM	El.magn. HF-Messungen/*-measurements*
FRI	Kluftzone/*Fracture zone investigation*
GS	Gebirgsspannungen/*Rock stresses*
HPA	Hydr. Parameter/*Hydr. parameters*
MI	Migration/*Migration*
MOD	Hydrodyn. Modellierung/*H. modeling*
NM	Neigungsmesser/*Tiltmeters*
UR	Untertageradar/*Underground radar*
US	Seismik/*Underground seismic testing*
VE	Ventilationstest/*Ventilation test*
WT	Wärmeversuch/*Heat test*

A — A Schnitt/*Section*

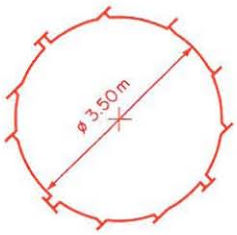

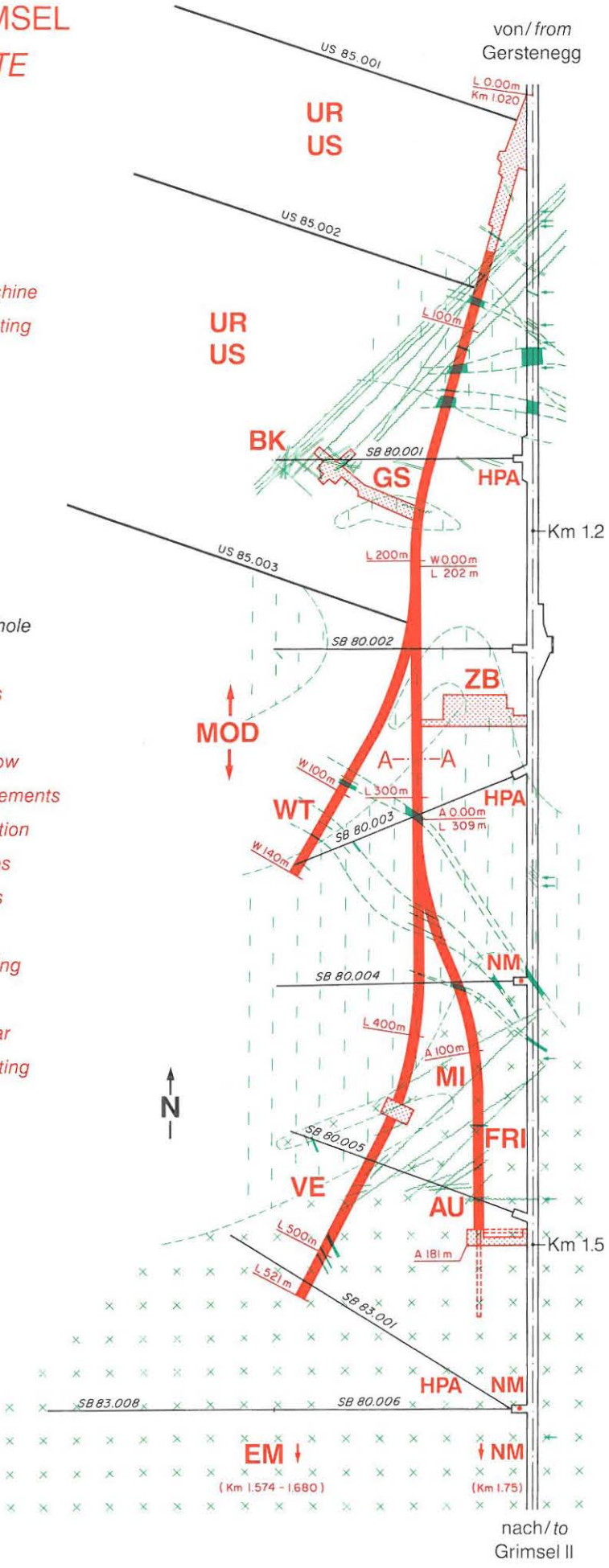

6/88

Preface

In the framework of its Waste Management Programme the Paul Scherrer Institute is performing work to increase the understanding of the geochemistry of nuclear waste relevant radionuclides. These investigations are performed in close cooperation with, and with the financial support of NAGRA. The present report is issued simultaneously as a PSI Report and a NAGRA NTB.

Contents

Abstract

Within the migration experiment at the Grimsel Test Site (GTS) various breakthrough tests, including non-sorbing as well as reactive tracers, are performed in a single fracture. During a special experiment, the water naturally flowing in the migration fracture (MI–water), was replaced by a groundwater of a somewhat different chemical composition (EM–water), which was pumped from borehole BOEM 85.012 located 200 m south of the migration site. The dipole flow field for this breakthrough experiment was established between borehole BOMI 86.004 (injection well) and borehole BOMI 87.006 (extraction well). The initial objective of this hydrogeochemical equilibrium test was to observe how the system responded to the injection of a "foreign" water and to determine the time required to reach new steady state conditions. A total of 22 water samples were taken from the extraction well for subsequent laboratory analyses. This test was part of the necessary preparation work required for future tracer migration experiments in which it might be necessary to inject a water with a different chemistry if a constant supply of natural migration water in the quantities required can not be guaranteed over the anticipated experimental time scales.

The results of the hydrogeochemical equilibration test showed clearly that anions such as F^- and Cl^- reached steady state concentrations in the extracted water within $\sim$ 50 hours whereas the major cations, Na^+ and Ca^{2+} required $\sim$ 150 hours. The three cations, Sr^{2+}, K^+ and Mg^{2+} showed evidence of being retarded more strongly. Sr^{2+} did not reach steady state until after $\sim$ 250 hours and K^+ and Mg^{2+} appeard to be still increasing slowly when the experiment was terminated after $\sim$ 312 hours. The conclusion from this first part of the work was that EM–water should not be used as a source of injection water in any future migration experiment with sorbing tracers.

These data were further analysed and interpreted assuming that the protomylonite fracture material behaves as a weak cation exchange medium giving rise to composition changes in the extracted water in addition to those resulting from simple mixing processes.

From the concentration–time data for the extracted water, curves representing the "interaction" component of the "foreign" water with the fracture material could be deduced. These results, together with selectivity coefficients for the major ions with respect to Ca^{2+}, and some simple assumptions concerning the fracture geometry, enabled a cation exchange capacity for the fracture material to be estimated. Using the estimated CEC value, in situ K_d values for Na^+ and Sr^{2+} were predicted. The sorption characteristics of Na^+ and Sr^{2+} are of direct relevance to the NAGRA/PSI programme at the GTS since field migration experiments with radioisotopes of both of these tracers are being carried out during 1990/1991.

Zusammenfassung

Innerhalb einer ausgewählten Einzelkluft im Felslabor Grimsel finden im Rahmen des Migrationsversuches Durchbruchtests mit konservativen und sorbierenden Tracern statt. In einem speziellen Experiment wurde das natürliche Kluftwasser (MI-Wasser) durch ein Grundwasser (EM-Wasser), welches eine zu MI-Wasser chemisch verschiedene Zusammensetzung aufweist, verdrängt. Das EM-Wasser wurde aus einer 200 m südlich zum Migrationstandort entfernten Bohrung (BOEM 85.012) entnommen. Zur Durchführung dieses Durchbruchversuches wurde ein Dipolfeld zwischen den Bohrlöchern BOMI 86.004 und BOMI 87.006 eingestellt. Das ursprüngliche Ziel dieses Versuches war es daher, herauszufinden, wie das System auf die Eingabe eines "fremden" Wasser reagiert und welche Injektionszeit benötigt wird, bis sich in der Kluft wiederum ein chemisches Gleichgewicht einstellt. Um die zeitliche Veränderung der Wasserchemie zu erfassen, wurden extraktionsseitig Wasserproben entnommen und anschliessend auf ihre Zusammensetzung im Labor untersucht. Dieses Experiment umfasst einen Teil notwendiger Vorbereitungsarbeiten für zukünftige Migrationsversuche, falls es notwendig sein sollte, chemisch "fremde" Injektionswässer dann zu verwenden, wenn eine konstante Zufuhr von unkontaminiertem MI–Wasser über die experimentelle Zeit nicht garantiert werden kann.

Die Resultate zeigen deutlich, dass die Anionen im extrahierten Mischwasser bereits nach 50 Stunden ein lokales Gleichgewicht erreichten. Demgegenüber benötigten die Kationen Na^+ und Ca^{2+} etwa 150 Stunden. Eine Veränderung der Sr^{2+}–Konzentration wurde für etwa 250 Stunden beobachtet, während K^+ und Mg^{2+} auch nach Beendigung des Experiments nach 312 Stunden noch leicht ansteigende Werte verzeichneten. Es wird daher dringend empfohlen, bei Migrationsexperimenten mit sorbierenden Tracern kein EM–Injektionswasser zu verwenden.

Aufgrund einer weitergehenden Datenanalyse wurde gefolgert, dass sich das Kluftmaterial während des Experimentes als schwaches Kationaustauschmedium verhielt, weshalb – neben dem reinen Mischprozess zwischen beiden Wässern – die chemische Zusammensetzung leicht beeinflusst wurde.

Von dem Konzentrations–Zeit–Datenmaterial liessen sich Kurven extrahieren, welche quantitativ die Wechselwirkung des "fremden" Wassers mit dem Kluftmaterial anzeigten. Mit Hilfe dieser Resultate, Labordaten von Selektivitätskoeffizienten der gemessenen Kationen gegenüber Ca^{2+} und einer Abschätzung der Kluftgeometrie liess sich die Kationenaustauschkapazität des Kluftmaterials grob berechnen. Unter Zuhilfenahme der berechneten CEC war es ferner möglich, in situ K_d–Werte für Na^+ und Sr^{2+} abzuschätzen. Die Untersuchung des Sorptionsverhaltens von Na^+ und Sr^{2+} umfasst einen wichtigen Teil der Feldarbeiten, welche im Rahmen der NAGRA/PSI Programmes Felslabor Grimsel durchgeführt werden. Während der Jahre 1990/91 laufen Migrationsversuche mit ^{22}Na und ^{85}Sr im Felslabor.

Résumé

Un essai de migration par injection continue a été éffectué au laboratoire souterrain du Grimsel (LSG) dans la fissure AU 96. Pour l'injection, une eau étrangère (eau EM), qui est chimiquement differente de l'eau interstitielle (eau MI) a été utilisée. Un champ dipôlair a été établi entre deux puits de forage dans la zone de migration, c'est-à-dire entre le forage d'injection (BOMI 86.004) et le forage d'extraction (BOMI 87.006).

Un des buts principaux de ce test d'équilibre hydrogéochimique était d'observer le comportement de ce système après l'injection d'une eau "étrangère", et de déterminer le temps nécessaire pour établir conditous stationnaires dans la zone de migration.

En total, 22 échantillons d'eau ont été prélevés dans le forage d'extraction et analysés en laboratoire. Cet essai fait parti des préparatifs nécessaires pour les essais futurs sur la migration des radionucléides dans la roche cristalline, car il n'est pas sur si l'eau de migration naturelle peut garantir un flux constant et suffisant dans certains expériments à long terme.

Les résultats de l'essai d'équilibration hydrogéochimique ont clairement montré que des anions comme F^-, Cl^- atteign des concentrations stationnaires dans le puit d'extraction après environ 50 heures. Par contre, les concentrations des cations majeurs, Na^+ et Ca^{2+} deviennent stationnaires après $\sim$ 150 heures. La retardation des cations Sr^{2+}, K^+ et Mg^{2+} est encore plus forte. Sr^{2+} one parvient á l'équilibre qu'après environ 250 heures tandis que les concentrations de K^+ et Mg^{2+} étaient toujours en légère augmentation après la conclusion de l'expérience ($\sim$ 312 heures). La conclusion à tirer est que l'on ne peut pas utiliser une eau "étrangère" comme eau de source pour l'injection des traceurs sorbents dans les essais de migration LSG.

Les résultats sont ensuite analysés et interprétés tenant compte que le remplissage de la faille se comporte comme un faible èchangeur de cations, qui est responsable pour des changements chimiques dans l'eau d'extraction en addition des changements qui résultent de mélangement avec l'eau étrangère.

D'après les mesures de concentration en fonction du temps au forage d'extraction, on a déduit des courbes de différence qui représentent l'interaction de l'eau étrangère avec le remplissage de la fissure. Les résultats, avec des coéfficients de sélectivité et des hypothèses sur la géométrie de la faille, ont permis d'estimer la capacité d'échange cationique (CEC) du remplissage minéral de la faille de migration. En utilisant la CEC estimée, les constantes de distribution (K_d) pour Na^+ et Sr^{2+} ont étées prédites.

Les propriétés de sorption de Na^+ et Sr^{2+} sont importantes pour le programme realisé dans le laboratiore souterrain de la Cédra/PSI au Grimsel, puisque ces deux traceurs sont utilisés dans des essais sur la migration des radionucléides en 1990/1991.

1 Introduction

Since the spring of 1988 PSI and NAGRA have been carrying out radioactive tracer migration experiments in the underground research laboratory at the Grimsel Test Site (GTS). Part of the main aims of the work is to investigate processes determining radionuclide migration in fractured media and to test radionuclide transport models (Hadermann and Roesel, 1985, Hadermann et al. 1988, Jakob et al. 1989). Migration experiments are being performed in a water bearing shearzone intersected by 10 boreholes equipped with multiple packers (Frick et al., 1988; McKinley et al., 1988; Hoehn et al., 1990). In the region of interest, i.e. within 10 m of the drift wall, this shear zone is essentially a two dimensional fault containing unconsolidated infill material. The whole fracture material exhibits a bulk chemical composition and mineralogy very close to the surrounding granitic bed rock. Geological and mineralogical characterisations of the fracture zone have been reported by Meyer et al. (1989). In addition, a structural description of the site is given in Bossart and Mazurek (1990).

Most of the migration experiments are conducted in two–well injection–extraction tests (doublet arrangement). In these tests, the dipole field is established by continuously pumping water into an injection well and simultaneously extracting water at a withdrawal well (see Figure 1). In the planning phase for the first migration experiments, the initial estimates indicated that injection and extraction flow rates of between 200 and 2000 ml min^{-1} might be required in order to establish a flow field which allow 100% tracer recovery. Complete recovery of the tracer was a criterion set for the experimental work since a mass balance in the system was considered essential for the subsequent modelling work. The need for such high injection rates, however, caused certain difficulties. The storage of groundwater naturally flowing out of the migration fracture into the drift (MI–water) was considered but then rejected since it was uncertain as to whether the groundwater chemistry of the large volumes required could be held constant over long times particularly with respect to P_{CO_2} and P_{O_2}. Pumping out water at the rates foreseen from any borehole capable of providing enough water would have disturbed the dipole flow field and there was the additional possibility of tracer cross contamination.

Therefore, groundwater from a borehole located about 300 m along the drift from the migration fracture was considered instead (EM–water). This groundwater (taken from borehole BOEM 85–012) is chemically different to MI–water (Bajo et al. 1987). Because of the differences in chemical composition, the EM–water was unlikely to be in equilibrium with the migration fracture material. However, an essential pre–requisite

for any migration tests with sorbing species is that the groundwater and fracture material are in chemical equilibrium. This is particularly important for the first set of sorbing tracers chosen (^{22}Na, ^{24}Na and ^{85}Sr). These cations were predicted to sorb linearly and reversibly on the protomylonite material via a cation exchange mechanism (Bradbury and Baeyens, 1989). The magnitude of their K_d–values depends on the relative ion occupancies on the small fraction of sheet silica minerals contained in the protomylonite. These ion occupancies are strongly dependent on the water chemistry (Baeyens et al. 1989).

In view of this, a long term dipole experiment consisting of a step input of EM–water in borehole BOMI 86.004 (subsequently referred as borehole 4) and the monitoring of the water chemistry in the extraction borehole BOMI 87.006 (subsequently referred as borehole 6) was performed to determine the time scale the system required to adjust to a new "equilibrium" state and to characterise the new conditions. The details of the methodology and the results of the test form the first part of this report.

Upon closer examination, the results proved to be sufficiently interesting to warrant an attempt to analyse them further than was initially foreseen in terms of some important physico–chemical fracture material characteristics. However, it should be stated that the experiments were not designed with this in mind, and in this respect the quality and quantity of the data are not optimal. Also, the estimates presented in the second part of the report required certain assumptions to be made, and some key parameter values were obtained from other studies carried out within the framework of the Grimsel migration experimental programme. Nevertheless, the analytical procedures and the estimates did provide some insight into the behaviour of the in situ system during a massive rock–water interaction experiment. The deductions should be viewed as first estimates which may be useful in the later planning and/or interpretation of migration experimental results even if only to provide a bound on likely parameter ranges.

For convenience, and in order to be consistent with the nomenclature adopted in previous reports, the term "mylonite" was taken here to describe the fracture material from location AU 126m. This material is used in all laboratory experiments. The term "protomylonite" refers to the migration fracture material (location AU 96m).

2 Experimental

2.1 On–line measurements

A dipole flow field was established between boreholes 4 (injection) and 6 (extraction) by using an injection flow rate, Q_i, of 45 ml min^{-1} and an extraction flow rate, Q_e of 105 ml min^{-1}. These flow rates were chosen on the basis of experience from previous migration experiments which yielded a 100% recovery of the injected tracers ^{82}Br, uranine and ^{4}He (see Eikenberg and Kipfer, 1989, Frick, 1990).

The experimental arrangement is schematically illustrated in Figure 1. The packer systems installed in the migration test boreholes were instrumented to allow on–line measurements of the pressures downhole. A constant injection flow rate of EM–water was attained by pressure regulation of the natural pressure difference between the borehole and the drift. In the tunnel, at both the injection and extraction sites, the water flow rates, O_2–content, pH and electrical conductivities were measured. The data from all probes were stored on a data acquisition system linked to an IBM–PC which allowed the signals from all devices to be logged and displayed graphically via an analogue to digital converter. More details concerning the experimental arrangement are given by Thorne (1990).

2.2 Groundwater analyses

During the experiment, which lasted 312 hours, 22 water samples were taken on the extraction side after the groundwater has passed through the analytical instruments. One sample of EM injection water was taken from borehole BOEM 85–012.

Groundwater samples were collected in 1 litre–polyethylene bottles which were first flushed with the groundwater and then filled to the brim in order to exclude, as far as possible, any air contamination. After the sampling campaign all bottles were brought to PSI for subsequent analyses of Na, K, Ca, Mg, Sr, Si_{tot}, F^-, Cl^-, SO_4^{2-}, alkalinity ($HCO_3^-/CO_3^{2-}/H_3SiO_4^-$) and pH. Cations were measured by atomic adsorption spectrometry, F^-, Cl^- and SO_4^{2-} by ion chromatography, pH by a glass electrode and the alkalinity by titration. More details concerning these standard analytical procedures can be found in the work of Bajo et al. (1987).

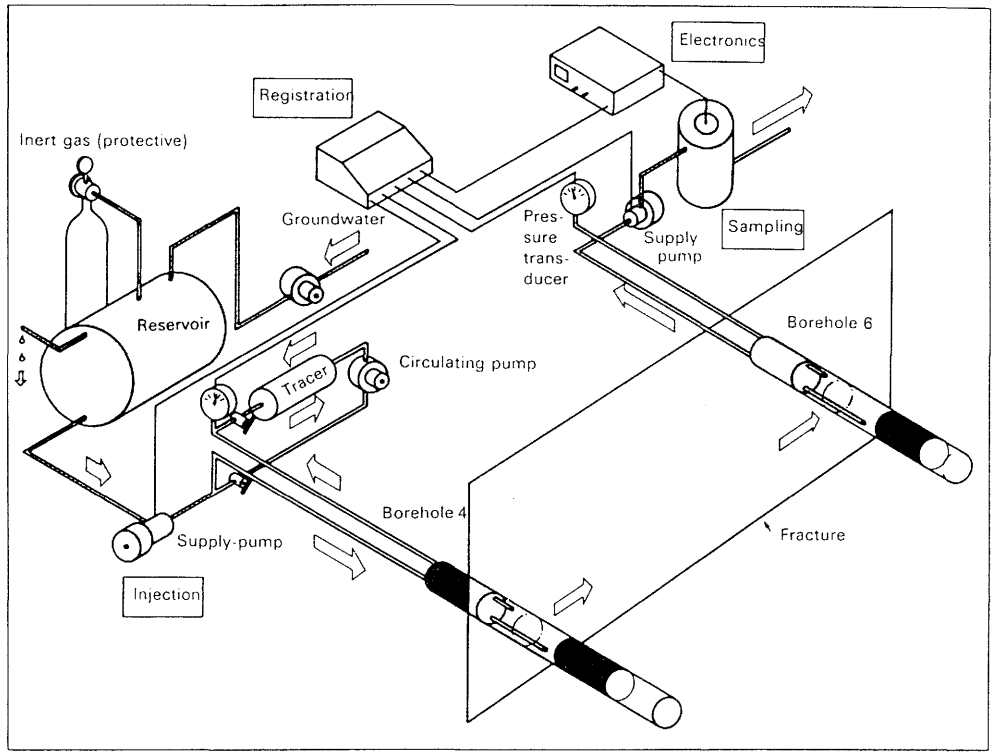

Figure 1: Schematic experimental arrangement for the EM water injection test between boreholes 4 and 6 (from Frick et al. 1988).

3 Experimental Results

3.1 Results of on–line measurements

The pH, electrical conductivity (E.C.) and oxygen (O_2) were monitored on–line on both the injection and extraction sides of the test arrangement. Table 1 presents data for (i) the EM–water at the injection well, (ii) MI–water recovered at the extraction well during the first few hours of the experiment and (iii) the mixed water at the end of the test.

Table 1: Results for the on–line measured parameters: oxygen content, pH and electrical conductivity at the injection and extraction wells.

Parameter	Injection well	Extraction well	
	EM–water	MI–water	MI/EM mixed water (after 312 hours)
pH	8.9 ± 0.1	9.5 ± 0.1*	9.4 ± 1*
E.C. [μS/cm]	78 ± 1.0	106 ± 1.0	94 ± 1.0
O_2 [ppm]**	< 0.1	< 0.1	< 0.1

* Laboratory determinations
** Detection limit ≈ 0.1 ppm

These parameters were measured for the following reasons:

1. To monitor possible air contamination and chemical changes in the injected EM–water (Note that the EM water was transported through a 300 m long polyamide pipe from its source to the injection well).

2. The changes in electrical conductivity on the extraction side was used as a "global" indicator for taking water samples over the most important time periods during

the experiment i.e. at times of maximum change. On–line pH measurements were also foreseen for this purpose but the electrode on the extraction side failed during the early stages of the experiment and the values given in Table 1 are laboratory measurements on collected samples.

The on–line measurements of the injected EM–water showed that the pH and electrical conductivity remained constant throughout the test and that the O_2 concentration was always below the detection limit of 0.1 ppm. The measured pH of the EM–water on the injection site was 8.9 $\pm$ 0.1 which was in good agreement with the previous measurements of Bajo et al. (1987). These results implied that no significant air contamination and/or changes in pH occurred during pumping of the EM–water into borehole 4.

The initial water extracted from borehole 6 exhibited an O_2 level of about 5 ppm which rapidly decreased within one hour to levels below the 0.1 ppm detection limit of the oxygen meter. The most probable origin of the oxygen was air contamination of the stagnant water existing in the tubing leading from the packer in borehole 6 to the instrumentation. (This water was not flushed out prior to starting the tests.) The pH and electrical conductivity reached values of 9.4 and 94 μS cm^{-1} respectively within the first $\sim$ 100 hours and thereafter remained constant within experimental error.

3.2 Laboratory analytical results of sampled water

The results of the chemical analyses of the major cations, anions, pH and alkalinity as a function of time are listed in Table 2. In Table 3 a summary of the water chemistry data available for the end members MI–water and EM–water is given.

The MI (2) data (Table 3) was calculated from the mean of the first 3 water sample analyses given in Table 2 under the assumption that the water which first emerged from the fracture was "pure" MI–water with no noteworthy admixture of EM–water occurring in this collection time period. Note that previous tests with non–sorbing tracers, carried out under similar flow field conditions, indicated that "first breakthroughs" occurred after $\sim$ 3 hours. The ionic composition of the MI–water calculated on this basis as well as the pH, alkalinity and electrical conductivity are in reasonably good agreement with the previous results from Bajo et al. (1989a) denoted by MI(1) in Table 3. Since no reliable water chemistry measurements for the EM–water were obtained during this

test (contamination of the EM–water sample) data from Bajo et al. (1987) are given in Table 3.

Table 2: Analytical results for the extracted water, pH and alkalinity as a function of time.

Sample No	time [h]	pH	alkalinity	Mg μeq/l	Ca μeq/l	Sr μeq/l	Na μeq/l	K μeq/l	F^- μeq/l	Cl^- μeq/l	SO_4^{2-} μeq/l
1	1	9.37	450	1.20	283	3.90	700	5.03	–	–	–
2	1.5	9.50	450	1.20	282	3.94	689	5.19	363	170	62.5
3	2.8	9.52	450	1.30	286	3.92	689	5.11	347	147	59.4
4	3.5	9.50	450	1.30	287	3.95	689	5.70	337	158	64.6
5	5.5	9.50	500	1.32	294	4.06	670	4.99	300	158	63.5
6	6.5	9.50	500	1.40	298	4.13	639	4.96	252	107	54.3
7	7.5	9.45	500	1.40	300	4.15	635	4.91	274	116	59.4
8	8.5	9.46	510	1.40	306	4.22	626	5.09	263	110	61.5
9	11.0	9.44	510	1.40	317	4.38	617	4.86	242	99	55.2
10	12.5	9.40	520	1.40	322	4.45	592	4.88	247	101	58.3
11	28	9.42	520	1.49	336	4.68	570	5.04	242	96	58.3
12	30	9.38	520	1.40	338	4.72	570	5.50	237	93	57.3
13	43	9.32	520	1.66	348	4.81	552	5.65	231	93	56.3
14	48	9.34	530	1.66	349	4.86	548	6.34	237	96	60.4
15	78	9.35	530	1.74	350	4.86	544	6.98	228	93	55.2
16	120	9.37	530	2.32	357	5.02	522	8.31	221	84	54.2
17	144	9.37	520	2.57	359	5.09	530	8.52	216	84	54.2
18	170	9.37	530	2.57	358	5.11	522	8.87	205	77	51.0
19	194	9.37	520	2.65	360	5.13	522	9.67	211	82	51.0
20	220	9.38	520	2.74	358	5.15	526	9.62	211	82	45.8
21	288	9.38	520	2.82	359	5.17	526	9.95	231	93	57.3
22	312	9.37	520	2.89	358	5.19	526	10.00	231	90	55.2

Table 3: MI– and EM–water compositions

Parameter	[1]MI(1)	[2]MI(2)	[3]EM
Na [μeq/l]	692 $\pm$ 9	692 $\pm$ 6	264 $\pm$ 7
K [μeq/l]	3.84 $\pm$ 0.50	4.96 $\pm$ 0.22	24.0 $\pm$ 0.8
Mg [μeq/l]	1.08 $\pm$ 0.25	1.24 $\pm$ 0.06	7.74 $\pm$ 0.16
Ca [μeq/l]	254 $\pm$ 2	284 $\pm$ 1	422 $\pm$ 11
Sr [μeq/l]	3.67 $\pm$ 0.04	3.92 $\pm$ 0.02	7.76 $\pm$ 0.23
SO_4^{2-} [μeq/l]	115 $\pm$ 11	118 $\pm$ 16	88 $\pm$ 20
F^- [μeq/l]	330 $\pm$ 5	355 $\pm$ 19	77.9 $\pm$ 4.2
Cl^- [μeq/l]	155 $\pm$ 8	158 $\pm$ 12	5.9 $\pm$ 1.1
pH	9.6 $\pm$ 0.1	9.5 $\pm$ 0.1	8.9 $\pm$ 0.1
Ionic Strength [M]	0.0012	0.0013	0.0010
Temperature [C]	12	12	12
Alkalinity [μeq/l]	420 $\pm$ 10	450 $\pm$ 10	600 $\pm$ 10
Conductivity [μS/cm]	103 $\pm$ 1	106 $\pm$ 1	75 $\pm$ 3

[1]MI(1): Mean values of 61 analyses taken at AU96 sampled over a ten month period from July 1986 to May 1987 (Bajo et al. 1989a).

[2]MI(2): Mean values of the first 3 samples of this experiment (sample numbers 1,2 and 3 of Table 2).

[3]EM: Mean values of 7 analyses from borehole 85–012 (Bajo et al. 1987).

3.2.1 Anions

The results for F^- and Cl^- are plotted in Figures 2 and 3 respectively. Although there is some scatter in the data, it can be seen that the concentrations of F^- (Figure 2a) and Cl^- (Figure 3a) remain constant for the first few hours at levels close to those in MI–water. The concentrations then decrease over a period of $\sim$ 50 hours and thereafter remain constant (see Figure 2b and 3b). Both the Cl^- and F^- concentrations appear to have reached steady state within the estimated experimental errors (see Table 4 in section 3.3 and Appendix). Considering the time scale of these experiments and the results of the speciation calculations given in a separate study (Eikenberg, 1989), it is anticipated that precipitation, dissolution and alteration reactions will have no significant influence on the overall Cl^- and F^- concentrations measured. Also, it is unlikely that

such anions will undergo interactions with the protomylonite material during the tests and they therefore behave as conservative water tracers. This statement is supported by experimental evidence from migration experiments in which another halide (^{82}Br) exhibited identical breakthrough curves to uranine (Frick, 1990).

3.2.2 Cations

The analytical results for the major cations, Na^+ and Ca^{2+}, and the trace cations, Sr^{2+}, K^+ and Mg^{2+}, are presented in Figures 4 – 8. Since the presence of ion pairs in these weakly mineralised waters ($I \cong 10^{-3}$ M) can be neglected to a first approximation, the data are given as cationic concentrations.

The cation undergoing the greatest absolute change in concentration is Na^+ which decreases from $\sim$ 690 μeq l^{-1} (MI–water) to a value of $\sim$ 530 μeq l^{-1} in the mixed water. The Na^+ concentration remains constant for the first few hours at the MI–water level and then falls continuously over a period of 150 – 175 hours before reaching a constant value for the remainder of the experimental time. The behaviour of Ca^{2+} is qualitatively very similar, reaching an apparently constant concentration on the same time scale as Na^+. In the case of Sr^{2+} there may be an indication of a continuing small increase with time after 150 hours. In contrast to Na^+ these two ions exhibit increasing concentrations with time since their levels in the injected water are greater than in the MI–water.

K^+ and Mg^{2+} show increasing concentration and also reach approximately constant (or very slightly rising) levels but on a time scale of $\sim$ 200 – 225 hours. Considering the experimental errors and the lack of data at longer times it is difficult to distinguish between a plateau and slowly rising values for the last few data points. The early time behaviour of K^+ and Mg^{2+} is very similar, but strikingly different from that of Na^+, Ca^{2+} and Sr^{2+} and the anions. Their initial concentrations remain constant at their respective levels in MI–water, as for the other ions in the system, but for a time period of $\sim$ 30 hours instead of $\sim$ 3 hours. The implication of this is that the trace cation K^+ and Mg^{2+} are interacting with the fracture material much more strongly than Na^+, Ca^{2+} and Sr^{2+}.

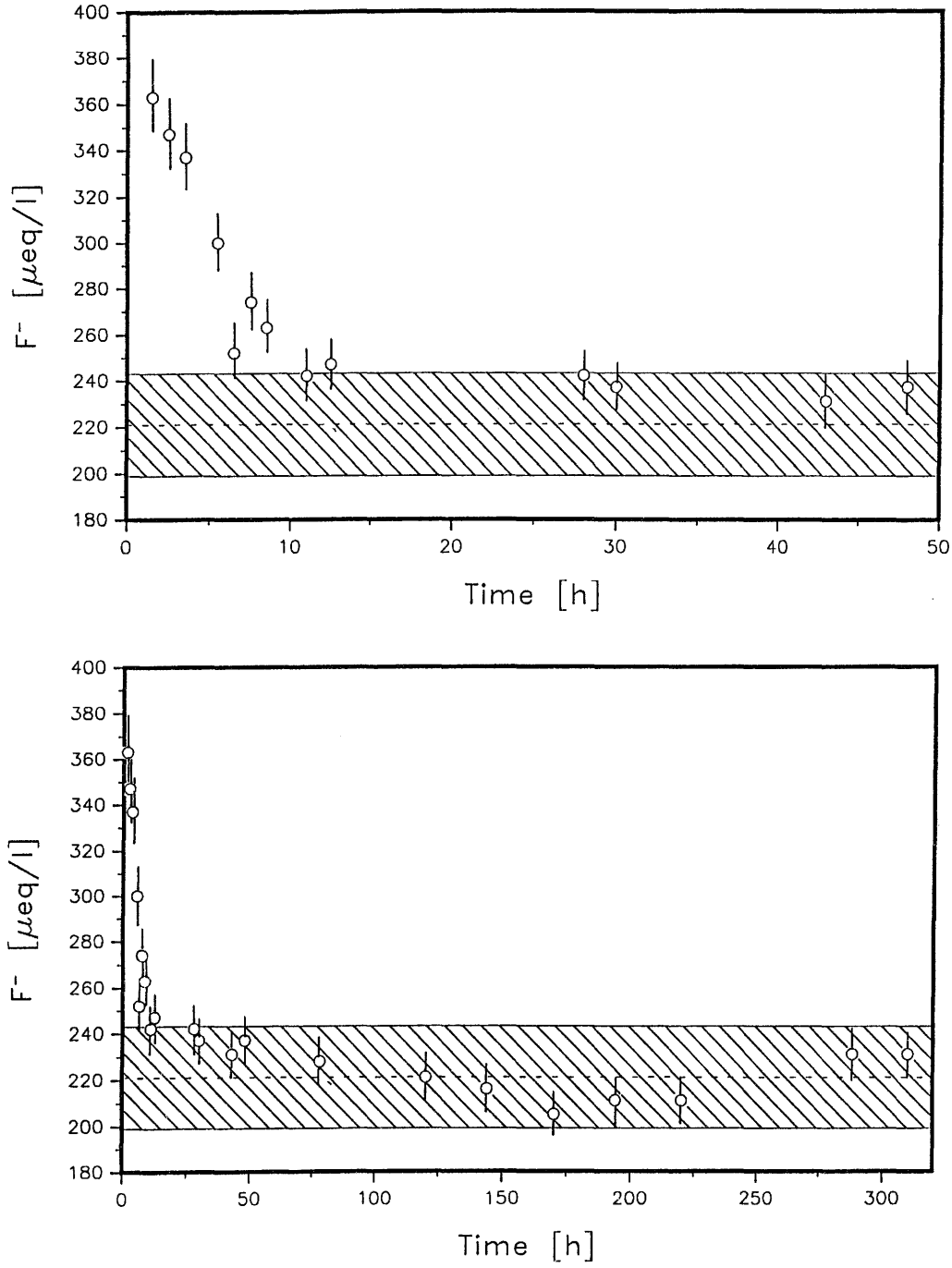

Figure 2: Concentrations of F^- as a function of time. A: early time data, B: complete data set. The dashed lines and cross hatches regions represent the calculated equilibrium concentrations in the extracted water (see Table 4 in section 3.3) and error bands (see Appendix) respectively.

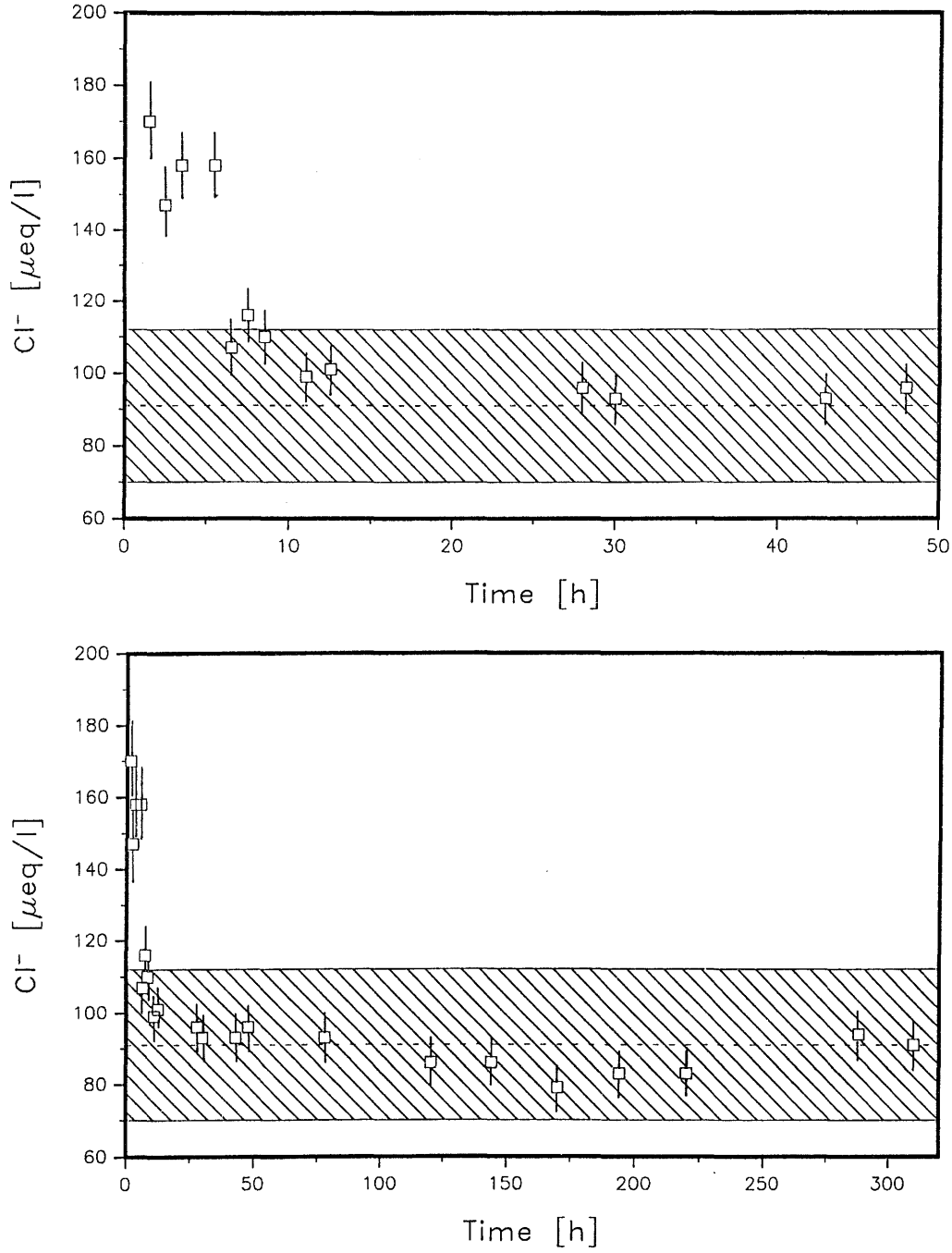

Figure 3: Concentrations of Cl^- as a function of time. A: early time data, B: complete data set. The dashed lines and cross hatches regions represent the calculated equilibrium concentrations in the extracted water (see Table 4 in section 3.3) and error bands (see Appendix) respectively.

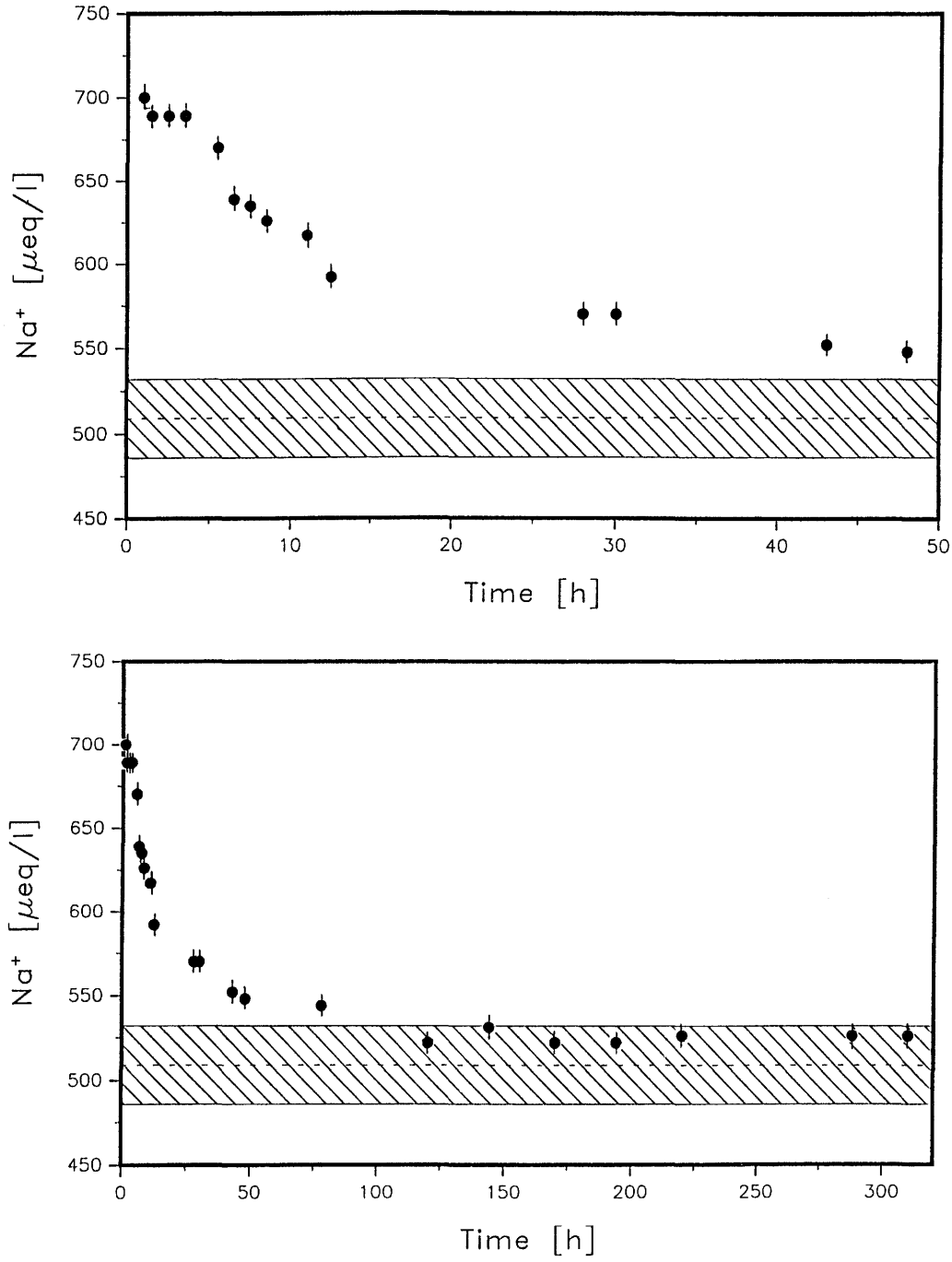

Figure 4: Concentrations of Na^+ as a function of time. A: early time data, B: complete data set. The dashed lines and cross hatches regions represent the calculated equilibrium concentrations in the extracted water (see Table 4 in section 3.3) and error bands (see Appendix) respectively.

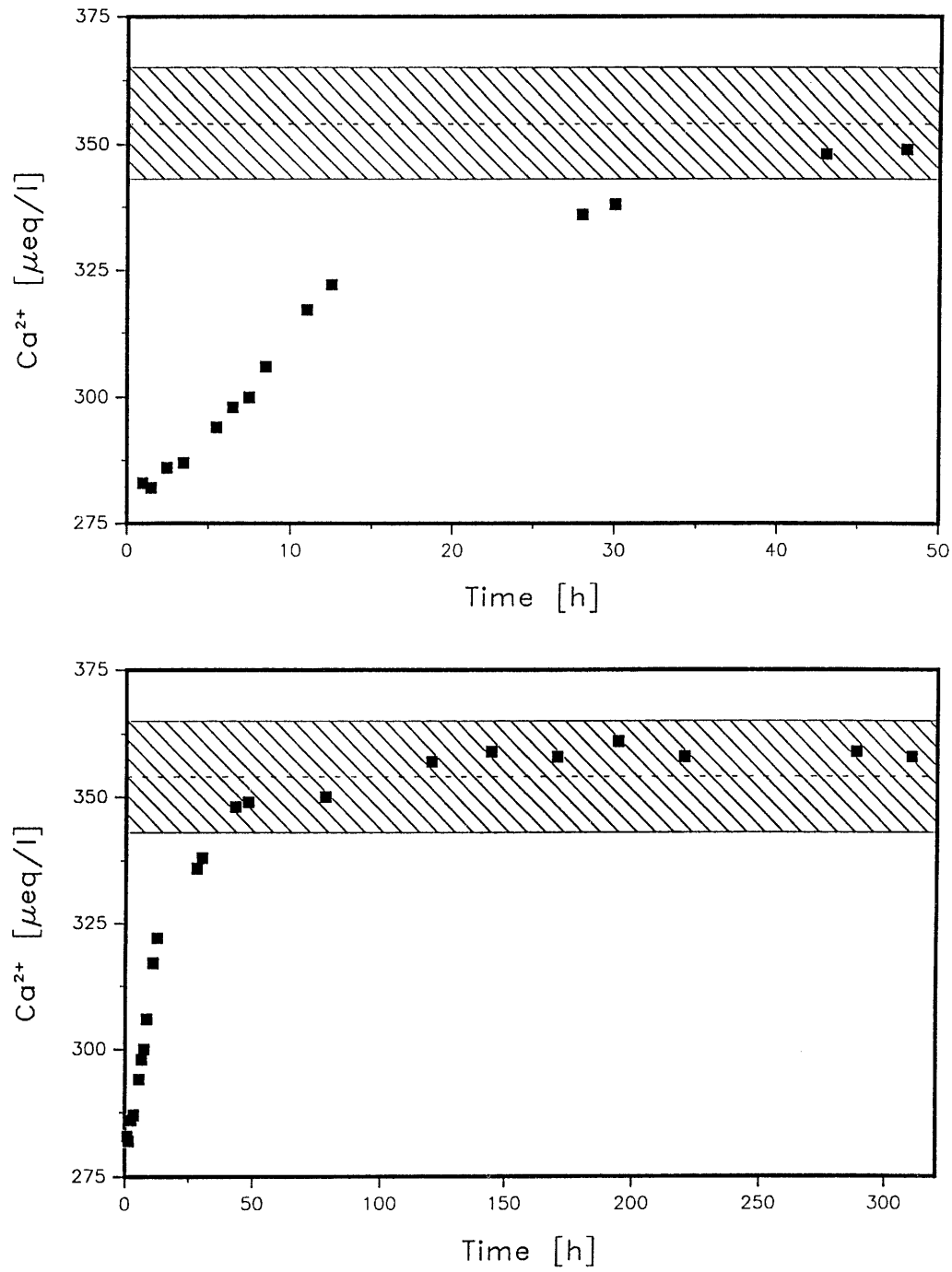

Figure 5: Concentrations of Ca^{2+} as a function of time. A: early time data, B: complete data set. The dashed lines and cross hatches regions represent the calculated equilibrium concentrations in the extracted water (see Table 4 in section 3.3) and error bands (see Appendix) respectively.

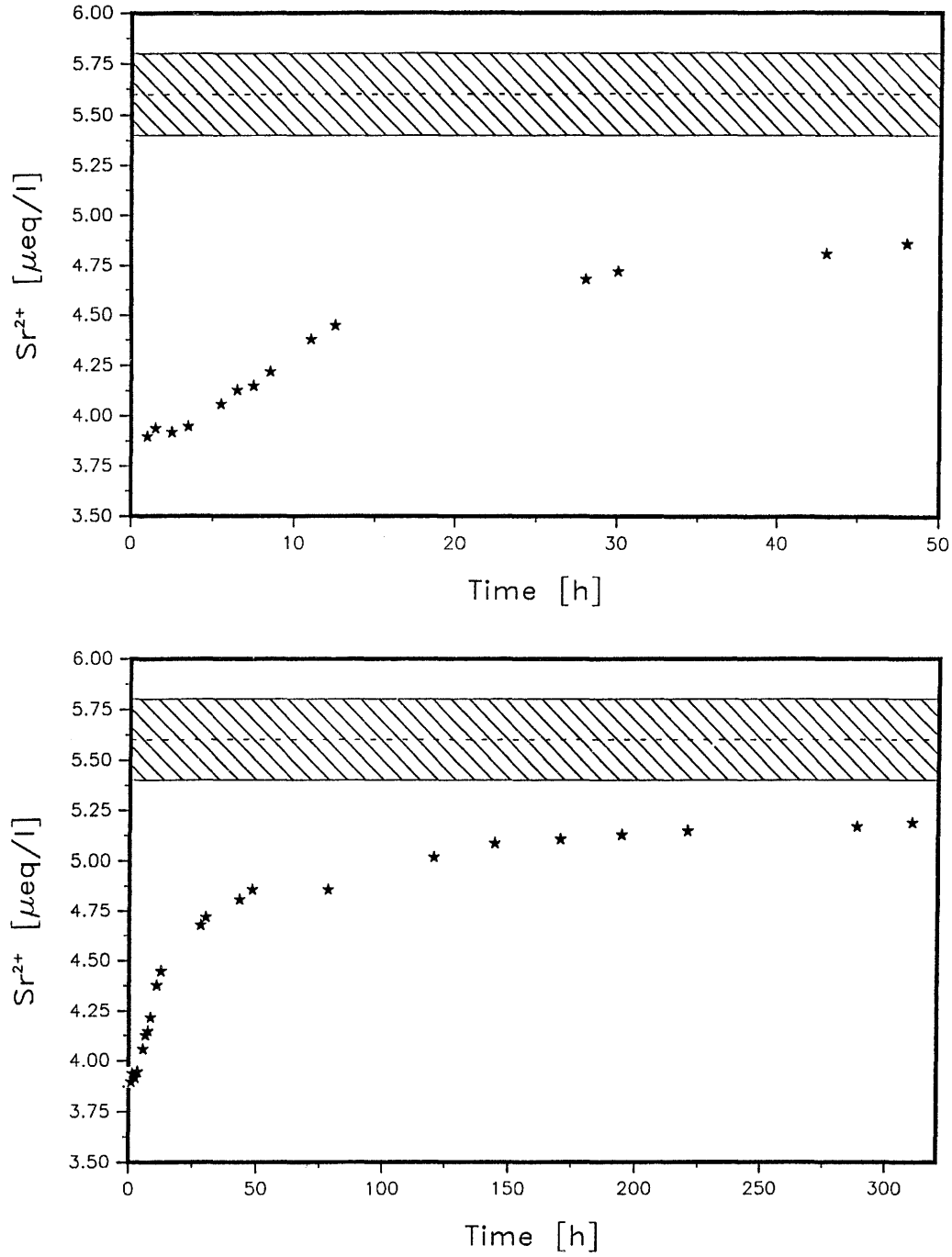

Figure 6: Concentrations of Sr^{2+} as a function of time. A: early time data, B: complete data set. The dashed lines and cross hatches regions represent the calculated equilibrium concentrations in the extracted water (see Table 4 in section 3.3) and error bands (see Appendix) respectively.

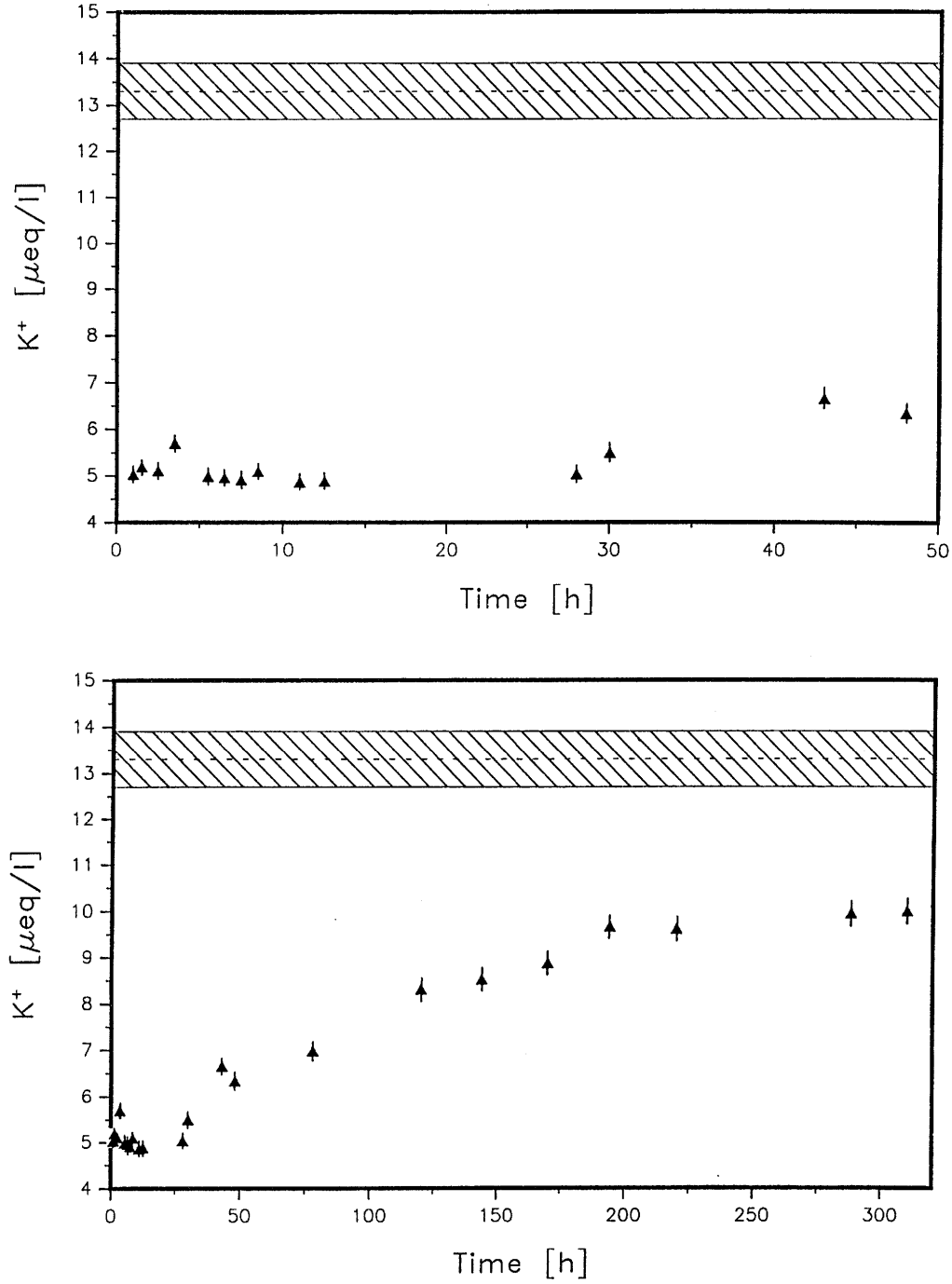

Figure 7: Concentrations of K^+ as a function of time. A: early time data, B: complete data set. The dashed lines and cross hatches regions represent the calculated equilibrium concentrations in the extracted water (see Table 4 in section 3.3) and error bands (see Appendix) respectively.

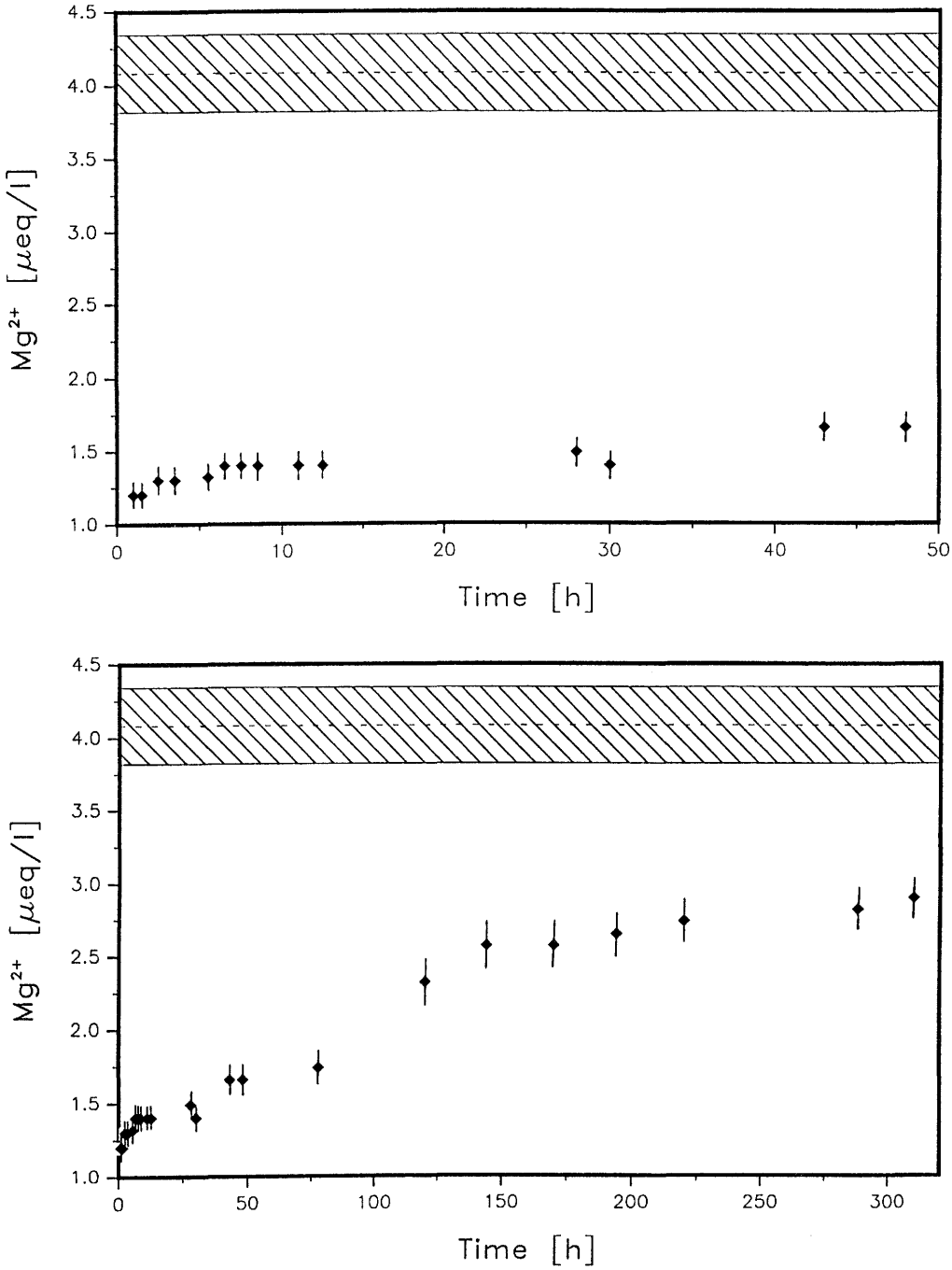

Figure 8: Concentrations of Mg^{2+} as a function of time. A: early time data, B: complete data set. The dashed lines and cross hatches regions represent the calculated equilibrium concentrations in the extracted water (see Table 4 in section 3.3) and error bands (see Appendix) respectively.

3.3 The mixing parameter X_i

If the injection and extraction rates (Q_i = 45 ml min^{-1} and Q_e = 105 ml min^{-1}, respectively) remain constant throughout the test, and mass is conserved, then the volume of water injected into borehole 4 will be recovered in borehole 6. The fractional contribution of the volume of water entering borehole 6 from the dipole flow field to the total extracted volume is then:

$$X_i = \frac{Q_i}{Q_e} = 0.43 \pm 0.01 \tag{1}$$

In the following, it is assumed that no significant mixing occurs between the injected EM–water and MI–water from outside the dipole flow along the flow paths from borehole 4 to borehole 6. This is a reasonable assumption since the natural pressure gradient between the two boreholes is small and the hydraulic conditions are almost wholly determined by the injection and extraction flow rates (see Herzog, 1989). This would imply that for the duration of the experiment only the injected water and the MI–water originally present within the dipole flow field determine the water composition in the fracture and that the admixture of MI–water occurs predominantly in the extraction borehole only. Note that the fracture volume involved is fixed by the geometry of the dipole field, which is also strongly dependent on Q_i and Q_e (see section 5.4.1). The above description of the system is presented pictorially in Figure 9.

It is important to realise that the volume fraction of the injection water, X_i, remains constant under the conditions specified above and, further, that the volume fraction of, and ion concentration in the MI–water drawn from outside the dipole flow field into the extraction well also remain constant. Therefore, the experimentally measured changes in concentrations in the water extracted from borehole 6 depend solely on the concentrations in the water flowing into borehole 6 from the dipole flow field.

Thus, if the measured concentration of any ion, B, in the extracted water at time t is, $C^B_{MIX}(t)$, then

$$C^B_{MIX}(t) = (1 - X_i)C^B_{MI} + X_i C^B_f(t) \tag{2}$$

where $(1 - X_i)$ is the volume fraction of MI–water in the extracted water and C^B_{MI} is the concentration of ion "B" in the MI–water. $C^B_f(t)$ is the concentration of ion "B" in the water entering borehole 6 **from** the dipole flow field. Note that $(1 - X_i)$, X_i

and C^B_{MI} are constants. Hence, if a steady state is reached at $t = t_{ss}$ for ion B, then it follows that

$$C^B_f(t) = C^B_F$$

where C^B_F is the concentration of B in the water flowing **in** the dipole flow field and

$$C^B_{MIX}(t_{ss}) = (1 - X_i)C^B_{MI} + X_i C^B_F \tag{3}$$

If the system reaches equilibrium, then C^B_F is equal to C^B_{EM}, where C^B_{EM} is the concentration of B in the injected EM–water.

Since the injection and extraction rates remained constant and the ion concentrations in MI– and EM–water are known, the composition of the mixed water at equilibrium can be calculated using equation 3. It is useful to compare the calculated equilibrium values with the "steady state" concentrations attained at the end of the experiment to obtain a measure of the "nearness to equilibrium" judged on this basis. The comparison is given in Table 4. Given the errors in the experimental values, it is reasonable to take equilibrium as being attained when the calculated and steady state concentrations are within $\pm$ 10 %. This appears to be the case for the cations Na^+, Ca^{2+} and Sr^{2+} and the anions Cl^-, F^- and SO_4^{2-}. For K^+ and Mg^{2+} the discrepancies are relatively large, $\sim$ 25% and 30% respectively. The concentration data for these two trace cations in MI–water are considered to be reliable (see Bajo et al, 1989). However, there is some uncertainty about their levels in the EM–water since differences in their concentrations of up to 40 % have been found between different series of measurements (unpublished data). This implies that their calculated equilibrium values given in Table 4 may be somewhat unreliable. Because of this, and since the measurements in this test were not continued for long enough, it is difficult to judge whether equilibrium has been reached for K^+ and Mg^{2+}. This point will be discussed again in section 5.1.

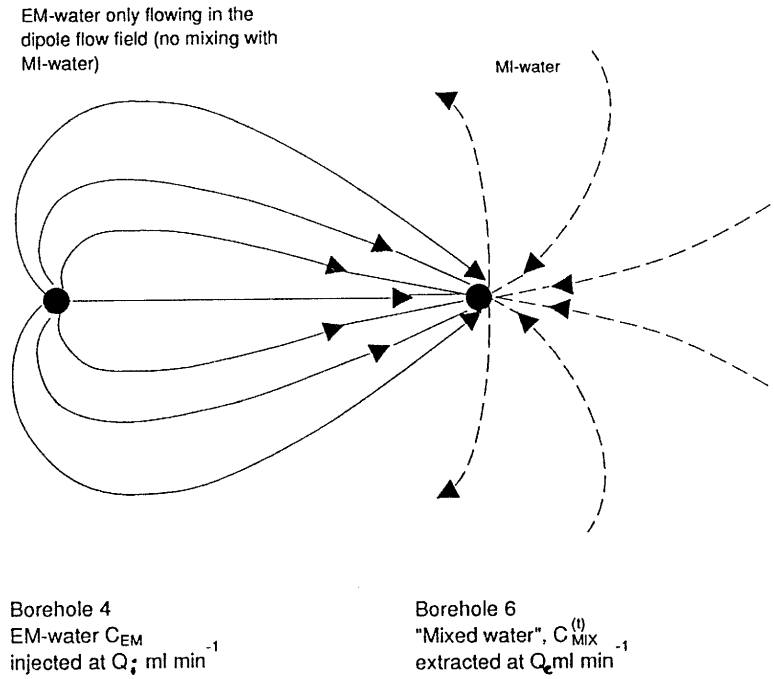

Figure 9: Schematic representation of the dipole flow field in the plane of the fracture between boreholes 4 and 6, assuming a homogenouesly transmissive 2-D aquifer..

Table 4: Comparison of the measured steady state concentrations and the calculated equilibrium composition of the extracted water using the data presented in Table 3.

	Calculated equilibrium concentration [μeq/l]	"Steady state" concentrations [μeq/l]	% Difference (%)
Na^+	509 $\pm$ 24	524 $\pm$ 4	3
Ca^{2+}	352 $\pm$ 12	358 $\pm$ 1	2
K^+	13.3 $\pm$ 0.6	10.0 $\pm$ 0.2	25
Mg^{2+}	4.1 $\pm$ 0.3	2.9 $\pm$ 0.1	29
Sr^{2+}	5.6 $\pm$ 0.2	5.2 $\pm$ 0.1	7
SO_4^{2-}	109 $\pm$ 25	108 $\pm$ 8	1
F^-	221 $\pm$ 23	226 $\pm$ 11	2
Cl^-	91 $\pm$ 21	88 $\pm$ 6	3

4 Ion Exchange Model

4.1 Background

A laboratory support programme is being carried out in parallel with the field migration studies at the Grimsel Test Site. Part of this programme involved a series of rock–water interaction experiments using fracture material from a fault intersecting the test drift at location AU 126m and MI–groundwater (Bajo et al., 1989b). It was found that by characterising the fracture material in terms of its cation exchange properties (Baeyens et al., 1989), the changes in the concentrations of the major ions Ca^{2+}, Na^{+}, Sr^{2+}, Mg^{2+} and K^{+} in the rock–water tests, under a variety of experimental conditions, could be quantitatively understood. The basic equations underlying cation exchange reactions are relatively simple. In general, a reversible cation exchange reaction involving the cations A and B, with valences z_A and z_B, respectively, can be expressed as:

$$z_B\,\overline{A} \;+\; z_A\,B \;=\; z_A\,\overline{B} \;+\; z_B\,A \tag{4}$$

in which the bars denote exchangeable ions on the surface of the cation exchange medium. A selectivity coefficient, K_c, which is a measure of the preference of the ion exchanger for a certain cation, can be defined for reaction (4) by the direct application of the mass-action law:

$$K_c \;=\; \frac{(N_B)^{z_A}[A]^{z_B}}{(N_A)^{z_B}[B]^{z_A}} \tag{5}$$

where [A] and [B] are the activities (or, to a first approximation, the molar concentrations) of ions A and B in solution. N_A and N_B are the fractional ion occupancies of the cations A and B on the solid phase and are defined as:

$$N_B \;=\; \frac{\overline{B}}{(\overline{A} \;+\; \overline{B})} \quad and \quad N_A \;=\; \frac{\overline{A}}{(\overline{A}+\overline{B})} \tag{6}$$

In a binary system the sum $(\overline{A} + \overline{B})$ normalised with respect to the mass of material, is equal to the cation exchange capacity.

In the following chapters, the aim is to use the experimental results given in Table 2 as a basis for obtaining an estimate of the CEC and ion occupancies of the protomylonite material in the migration fracture. From such data it is possible to make predictions of the likely "in situ" sorption of Na^{+} and Sr^{2+} assuming that their interactions with the protomylonite are determined predominantly by a cation exchange mechanism. In order to accomplish this, additional information is needed, principally selectivity coefficients.

From the results obtained in some previous laboratory rock water interaction experiments, selectivity coefficients for Na–Ca, K–Ca, Mg–Ca and Sr–Ca exchange reactions were calculated from of the water chemistry, and measured fractional ion occupancies using equation 5 (Baeyens and Bradbury, 1989). The values obtained, together with the data from which they were deduced, are summarised in Table 5. Strictly speaking, equation 5 is only valid for exchange reactions in a binary system whereas the fracture groundwater system is clearly multi–ionic. Since the K_c–value given will be used in later calculations some comments as to their applicability are required.

(i) Often, K_c values are not constant but depend on fractional ion occupancies. In order to fully characterise binary ion exchange reactions, K_c values need to be measured as a function of the ion occupancies (i.e. from $N_B = 0$ to $N_B = 1$) at constant ionic strength (Gaines and Thomas, 1953). The data available from the previous work (Table 5) extend only over a narrow range of fractional ion occupancies corresponding to the water compositions used in the tests. Consequently, the variation of K_c with N_B is unknown and the calculated K_c–values given in Table 5 cannot strictly be applied outside the composition ranges of the waters used.

(ii) The approach taken of considering the multi–ion system as a series of binary systems in which selectivity coefficients were calculated with respect to Ca^{2+}, is largely justified on the basis that Ca^{2+} is by far the dominant cation occupying the exchange medium. (The fractional ion occupancies of Ca^{2+} in the batch sorption experiment using rock–water ratios of 2:1, 1:2 and 1:10 lie in the region of 0.75). If Sr^{2+} and Mg^{2+} are considered to behave similarly to Ca^{2+}(see later), then the fractional occupancy of the bivalent ions is ~ 0.85.

(iii) By considering a series of binary exchange processes, it may appear that the influence of other competing ions is not taken into account. However, the selectivity coefficients given in Table 5 have to be considered as **empirical values** and the effect of any competitive exchange reactions are implicitely included. Ion occupancies were directly measured at equilibrium under a specific set of experimental conditions and used in the calculation of the K_c–values. The influence of any competitive effects from other ions in the system on the ion occupancies of the two ions being considered had already occurred and was consequently reflected in the occupancy values measured and hence in the K_c–value calculated. Thus, the K_c–values given in Table 5 only apply to this system and then only under the constraint given in (i) above.

Although this approach may not be entirely rigorous, its application led to a good quantitative description of the results in the previous study (see Bradbury (Ed.), 1989) and enabled predictions to be made for the sorption of trace quantities of active Sr^{2+} and Na^{+} which were largely confirmed in a later experimental programme (Aksoyoglu et al., 1990).

The selectivity coefficients for Na–Ca, Mg–Ca and Sr–Ca (Table 5) deviate by $\sim$ 25% about mean values of 1.1, 0.8 and 1.2 respectively, and show no significant trends with concentration. In view of the uncertainties in the experimental data and sample to sample variation, the three selectivity coefficients are considered to be in a good agreement with one another and a value of K_c = 1 is taken for each in the subsequent calculations. Inspection of Table 5 shows that in some cases the concentration range of these cations in the MI– and EM–waters is outside the experimental range. However, what is important here are the fractional occupancies and these vary weakly with concentration. Therefore, it is considered reasonable to assume that the K_c–values are valid for the MI– and EM–water concentration ranges.

The K–Ca exchange behaviour is different in that the selectivity coefficient is clearly a function of the K^{+} ion fractional occupancy, i.e. the selectivity coefficient increases with decreasing fractional occupancy/solution concentration in Table 5. The K^{+} concentrations in the MI– and EM–waters are both lower than the smallest concentration for which data are available from the laboratory measurements. (This is particularly so for the MI–water where the K^{+} levels are approximately 10 times lower). In these groundwaters the low K^{+} contents will most likely lead to fractional occupancies of only a few per cent. Neither fractional occupancies nor K–Ca selectivity data are available in the appropriate ranges and it is not possible, on the basis of the limited data available, to make a meaningful extrapolation. However, for the reasons given in the next section, it was desirable to include K^{+} in the calculations. A constant value of 360 was taken for the K–Ca selectivity coefficient (the highest value given in Table 5). The actual values in the range of K^{+} concentrations being considered could be higher.

Table 5: Selectivity coefficients of the major cations with respect to Ca^{2+} at different mylonite to water ratios (From Baeyens and Bradbury, 1989).

Rockwater Interaction experiment Solid:Liquid Ratio [g ml^{-1}]	Na			K			Mg			Sr			Ca	
	Quantity on mylonite [meq kg^{-1}]	Conc. in liquid [M]	$^{Na}_{Ca}K_c$	Quantity on mylonite [meq kg^{-1}]	Conc. in in liquid [M]	$^{K}_{Ca}K_c$	Quantity on mylonite [meq kg^{-1}]	Conc. in liquid [M]	$^{Mg}_{Ca}K_c$	Quantity on mylonite [meq kg^{-1}]	Conc. in liquid [M]	$^{Sr}_{Ca}K_c$	Quantity on mylonite [meq kg^{-1}]	Conc. in liquid [M]
2:1	1.9 1.9	1.3×10^{-3} 1.3×10^{-3}	1.04 0.99	6.5 6.9	7.0×10^{-4} 7.0×10^{-4}	37 38	2.6 2.8	7.5×10^{-5} 7.5×10^{-5}	0.55 0.58	0.4 0.4	8.0×10^{-6} 8.0×10^{-6}	0.84 0.86	30.8 31.5	4.9×10^{-4} 4.9×10^{-4}
1:2	1.8	7.9×10^{-4}	1.51	3.6	1.6×10^{-4}	153	1.6	1.5×10^{-5}	0.87	0.3	1.9×10^{-6}	1.33	23.3	1.9×10^{-4}
1:10	1.6 2.4	7.6×10^{-4} 7.1×10^{-4}	0.82 1.01	2.0 3.1	4.8×10^{-5} 5.4×10^{-5}	361 280	0.9 1.6	4.5×10^{-6} 6.0×10^{-6}	0.95 0.91	0.4 0.5	1.4×10^{-6} 1.3×10^{-6}	1.26 1.41	24.5 36.4	1.2×10^{-4} 1.3×10^{-4}
MI–Water	–	6.9×10^{-4}	–	–	5.0×10^{-6}	–	–	6.2×10^{-7}	–	–	2.0×10^{-6}	–	–	1.4×10^{-4}
EM–Water	–	2.6×10^{-4}	–	–	2.4×10^{-5}	–	–	3.9×10^{-6}	–	–	3.9×10^{-6}	–	–	2.2×10^{-4}

4.2 Ion occupancy calculations

The EM–water injection experiment is, in many respects, nothing more than a rock–water interaction test carried out on a large scale. The main difference is that laboratory measurements were performed in static batch tests and the field experiments in a fracture under dynamic conditions in a dipole flow field. The approach described here allows fractional occupancies on the fracture material to be estimated under certain simplifying assumptions which will be specified. Net changes in the fractional ion occupancies on the protomylonite can be calculated and related to the evolution of the measured water chemistries.

Inspection of the MI– and EM–water compositions in Table 3 reveals that the Na^+ plus Ca^+ concentrations, expressed on an equivalent scale, represent over 98 % of the cations present. For the laboratory experiments carried out at a liquid to solid ratio of 10:1, where the water composition is closest to those of the groundwaters, the Ca^{2+} plus Na^+ occupancies are $\sim$ 89 % of the total exchange capacity. The occupancies of Na^+ plus Ca^{2+} are expected to be even higher for protomylonite material in equilibrium with either of the two groundwaters since the concentrations of K^+, $Sr^{2+}$and $Mg^{2+}$are lower. Clearly, $Ca^{2+}$and Na^+ are the two most important cations in the system with respect to their concentrations in the groundwaters and their occupancies on the fracture material. However, it was considered neccessary to include K^+ separately in the following calculations because of its relatively high concentration in the EM–water and its high selectivity coefficient compared with the Na–Ca, Sr–Ca and Mg–Ca values.

In this treatment, the bivalent ions are considered together (see section 4.1) and the following exchange equilibria can be written:

$$M^{2+} - \text{protomylonite} + 2Na^+ \rightleftharpoons 2Na^+ - \text{protomylonite} + M^{2+} \quad (7)$$

$$M^{2+} - \text{protomylonite} + 2K^+ \rightleftharpoons 2K^+ - \text{protomylonite} + M^{2+} \quad (8)$$

where M^{2+} = Ca^{2+} + Sr^{2+} + Mg^{2+}.

The selectivity coefficient of Na^+ with respect to M^{2+} can be expressed as:

$$^{Na}_{M}K_c = \frac{N_{Na}^2 \cdot C_M}{N_M \cdot C_{Na}^2} \quad (9)$$

or

$$\frac{N_{Na}^2}{N_M} = \Theta_1 \tag{10}$$

where

$$\Theta_1 = \frac{C_{Na}^2}{C_M} \, {}^{Na}_{M}K_c \tag{11}$$

The selectivity coefficient of K^+ with respect to M^{2+} can be expressed as:

$${}^{K}_{M}K_c = \frac{N_K^2 \cdot C_M}{N_M \cdot C_K^2} \tag{12}$$

or

$$\frac{N_K^2}{N_M} = \Theta_2 \tag{13}$$

where

$$\Theta_2 = \frac{C_K^2}{C_M} \, {}^{K}_{M}K_c \tag{14}$$

Also

$$N_{Na} + N_K + N_M = 1 \tag{15}$$

Equations (10), (13) and (15) can be solved to yield expressions for N_{Na}, N_K and N_M i.e.

$$N_{Na} = \frac{-(1 + (\frac{\Theta_2}{\Theta_1})^{1/2}) \pm \sqrt{(1 + (\frac{\Theta_2}{\Theta_1})^{1/2})^2 + 4 \cdot \frac{1}{\Theta_1}}}{2 \cdot \frac{1}{\Theta_1}} \tag{16}$$

$$N_K = \frac{-(1 + (\frac{\Theta_1}{\Theta_2})^{1/2}) \pm \sqrt{(1 + (\frac{\Theta_1}{\Theta_2})^{1/2})^2 + 4 \cdot \frac{1}{\Theta_2}}}{2 \cdot \frac{1}{\Theta_2}} \tag{17}$$

$$N_M = 1 - (N_{Na} + N_K) \tag{18}$$

Using the K_c–values given in the previous section, it is interesting to compare the values of Θ_2/Θ_1 and $1/\Theta_1$ in equation (16) and Θ_1/Θ_2 and $1/\Theta_2$ in equation (17) for the two groundwaters. Table 6 shows for both waters that $\frac{1}{\Theta_1} \gg \frac{\Theta_2}{\Theta_1}$ (equation (16)), and $\frac{1}{\Theta_2} \gg \frac{\Theta_1}{\Theta_2}$ (equation (17)) and hence equations (16) and (17) can be approximated by

$$N_{Na} \sim \Theta_1^{1/2} \tag{19}$$

$$N_K \sim \Theta_2^{1/2} \tag{20}$$

Note that the negative solutions to equations (16) and (17) have no physical meaning.

Table 6: Θ_2/Θ_1 and $1/\Theta_1$ values (equation 16), Θ_1/Θ_2 and $1/\Theta_2$ values (equation 17) for MI– and EM–groundwaters. For both groundwaters the selectivities ${}^{Na}_{M}K_c$ and ${}^{K}_{M}K_c$ were taken as 1 and 360, respectively.

	MI–water	EM–water
$\frac{\Theta_2}{\Theta_1}$	$1.9 \cdot 10^{-2}$	$3.1 \cdot 10^{0}$
$\frac{1}{\Theta_1}$	$3.0 \cdot 10^{2}$	$3.4 \cdot 10^{3}$
$\frac{\Theta_1}{\Theta_2}$	$5.3 \cdot 10^{1}$	$3.2 \cdot 10^{-1}$
$\frac{1}{\Theta_2}$	$1.6 \cdot 10^{4}$	$1.1 \cdot 10^{3}$

The above implies that in the expression for N_{Na} (N_K) the cross–term which includes the influence of K–Ca exchange i.e. via $\frac{\Theta_2}{\Theta_1}$ (Na–Ca exchange i.e. via $\frac{\Theta_1}{\Theta_2}$) on the sodium (potassium) occupancy only have a second order effect and can be ignored to a first approximation. Though exchange reactions between Na^+ and K^+ have not been explicitly included, they are implicitly taken into account in equations (16) and (17) via the Θ_2/Θ_1, and Θ_1/Θ_2 terms respectively. This can be seen in the following way. From equations (11) and (14)

$$\frac{\Theta_1}{\Theta_2} = \frac{C_{Na}^2 \cdot {}^{Na}_{M}K_c}{C_M} \cdot \frac{C_M \cdot 1}{C_K^2 \cdot {}^{K}_{M}K_c} \tag{21}$$

$$= \frac{C_{Na}^2}{C_K^2} \cdot \frac{{}^{Na}_{M}K_c}{{}^{K}_{M}K_c} \tag{22}$$

and from equation (9) and (12)

$$\frac{{}^{Na}_{M}K_c}{{}^{K}_{M}K_c} = \frac{N_{Na}^2 \cdot C_K^2}{N_K^2 C_{Na}^2} = ({}^{Na}_{K}K_c)^2 \tag{23}$$

Hence

$$\frac{\Theta_1}{\Theta_2} = \left(\frac{C_{Na}}{C_K} \cdot {}^{Na}_{K}K_c\right)^2 \tag{24}$$

and similarly

$$\frac{\Theta_2}{\Theta_1} = \left(\frac{C_K}{C_{Na}} {}^{K}_{Na}K_c\right)^2 \tag{25}$$

Therefore, equations such as (16) and (17) expressed in terms of two of the variables i.e. ${}^{Na}_{M}K_c$ and ${}^{K}_{M}K_c$ implicitly include the influence of the third i.e. ${}^{K}_{Na}K_c$ (see for example Lewis and Thomas, 1953). For the particular conditions existing in this system, equation (25) yields a value for ${}^{K}_{Na}K_c$ of approximately 19 for MI– and EM–groundwaters in equilibrium with the protomylonite.

In this section equations have been derived relating the fractional ion occupancies of Na^+, K^+ and M^{2+} (= Ca^{2+} + Mg^{2+} +Sr^{2+}) on the protomylonite material to the concentrations of the cations in solution at equilibrium assuming ion exchange reactions only. Plausible values for Na–M and K–M selectivity coefficients have been given for compositions within the range covered by the MI– and EM–groundwaters.

For any water composition which is a mixture of MI– and EM–water, equations (19) and (20) yield the N_{Na} and N_K values, respectively, at equilibrium. Equation (18) yields the fractional occupancy of the bivalent ions from which the individual occupancies can be determined:

$$\frac{N_M}{C_M} \simeq \frac{N_{Ca}}{C_{Ca}} \simeq \frac{N_{Sr}}{C_{Sr}} \simeq \frac{N_{Mg}}{C_{Mg}} \tag{26}$$

(Assuming ${}^{Sr}_{Ca}K_c = {}^{Mg}_{Ca}K_c \simeq 1$, see section 4.1)

Hence, if the water composition in equilibrium with the protomylonite is known, the fractional ion occupancies $N_{Na}, N_K, N_{Ca}, N_{Mg}$ and N_{Sr} can be calculated.

5 Model Predictions and Evaluation of the Experimental Data

5.1 Composition of the water flowing in the fracture

Under the assumption that mass is conserved in the system, the concentrations of the individual cations and anions in the water entering borehole 6 from the dipole flow field can be calculated as a function of time using the data in Table 2 and equation 2. The calculated concentrations for the cations as a function of time are given in Table 7.

Table 7: Cation concentrations entering borehole 6 from the dipole flow field.

Time [h]	C_F^{Na} [μeq/l]	C_F^{Ca} [μeq/l]	C_F^{K} [μeq/l]	C_F^{Mg} [μeq/l]	C_F^{Sr} [μeq/l]
1	711	284	4.8	1.2	3.9
1.5	682	281	5.2	1.2	3.9
2.8	682	291	5.0	1.4	4.0
3.5	682	293	6.3	1.4	4.0
5.5	641	311	5.0	1.4	4.2
6.5	570	319	5.0	1.6	4.4
7.5	560	323	4.8	1.6	4.5
8.5	540	337	5.3	1.6	4.6
11.0	520	362	4.7	1.6	5.0
12.5	459	374	4.8	1.6	5.1
28	408	407	5.1	1.8	5.7
30	408	412	6.2	1.6	5.8
43	368	434	8.9	2.2	6.0
48	360	434	8.2	2.2	6.1
78	348	439	9.7	2.4	6.1
120	307	453	12.8	3.7	6.5
144	314	458	13.2	4.3	6.6
170	297	456	14.1	4.3	6.6
194	297	458	15.9	4.5	6.7
220	307	456	15.8	4.7	6.7
288	307	458	16.6	4.9	6.8
312	307	456	16.6	5.1	6.8

By referring to these values or to Figures 4 – 8, it can be seen that the major cations in the system (Na^+ and Ca^{2+}) appear to reach steady state values within $\sim$ 150 hours. The cations present at trace levels appear to exhibit slowly increasing concentrations up to the time at which the experiment was terminated. Since the anions were essentially at steady state after only $\sim$ 50 hours (see Figures 2 and 3), then, stricly speaking, either all the cations are at steady state or none are. The most likely situation is that none of the cations have reached their steady state values and the system is still evolving slowly. However, at times greater than $\sim$ 225 hours the rates of change in the concentrations are extremely slow (see for example Figure 8 for Mg^{2+}). It is therefore reasonable to assume that the concentrations calculated in Table 7 at the end of the experiment are close to those **flowing in the dipole flow field.** The water composition obtained on this basis (Table 8) will be used in the calculations presented in the following sections.

Table 8: Cation composition of the water flowing **in the fracture** assuming steady state conditions have been reached at the end of the experiment (see text).

Cation	Concentration [μeq/l]
Na^+	305 $\pm$ 6
Ca^{2+}	456 $\pm$ 3
Sr^{2+}	6.8 $\pm$ 0.1
K^+	$\geq$ 16.6
Mg^{2+}	$\geq$ 5.1

5.2 Model predictions

In the following calculation it is assumed that the fracture material is initially in equilibrium with MI–water having the composition given in Table 3, MI(2). When water of a different composition is injected into the fracture via borehole 4, a conditioning process takes place in which the fracture material within the dipole flow field gradually tends to equilibrate with the "foreign" injected water. The premiss here is that the main mechanism involved in the conditioning process is cation exchange where the fractional cation occupancies on the fracture material are governed by the water composition, the selectivity coefficients given in Table 5 and the equations derived in section 4.2. The fractional ion occupancies will change from their initial values, corresponding

to equilibrium between protomylonite and MI–water, to new values corresponding to equilibrium between protomylonite and the water composition present in the fracture at the end of the test (see Table 8). The calculated fractional ion occupancies relating to these two conditions are given in Table 9.

Table 9: Calculated fractional cation occupancies (N_B) on the protomylonite in equilibrium with MI–water and in equilibrium with the steady state water composition flowing in the fracture.

	MI–water composition (Table 3, MI(2)) N_B	Steady state water composition (Table 8) N_B	Change in ion occupancy ΔN_B
Na^+	0.060	0.020	–0.040
Ca^{2+}	0.910	0.925	+0.015
K^+	0.010	0.031	+0.018
Mg^{2+}	0.004	0.010	+0.006
Sr^{2+}	0.013	0.014	+0.001

With regard to this table the following comments can be made:

(i) If the two major cations in the system (Na^+ and Ca^{2+}) are considered, then the calculated N_B values for the two waters indicate that the fractional occupancy of Na^+ should decrease ($\Delta N_{Na} \simeq$ –0.04) and the occupancy of Ca^{2+} should increase ($\Delta N_{Ca} \simeq$ +0.015). Thus, a first prediction of the model is that during the course of the experiment Na^+ should "de–sorb" and thus deliver Na^+ to the aqueous phase, whereas Ca^{2+} should exhibit the opposite behaviour. If ion exchange is the dominate mechanism, then the "gains" and "losses" of Na^+ and Ca^{2+} respectively in the aqueous phase should be equal to the product of the corresponding ΔN_B–value and the total cation exchange capacity of the mass of in situ fracture material.

(ii) Although present only at trace levels K^+ shows a positive change in its fractional occupancy ($\Delta N_K \simeq$ + 0.018) of approximately the same magnitude as Ca^{2+}. The explanation for this is that the K^+ concentrations change by a factor of three and the selectivity coefficient of K^+ with respect to the bivalent ions is large.

(iii) The fractional occupancy changes for Sr^{2+} and Mg^{2+} are relatively small

($\Delta N_{Sr} \simeq$ + 0.001 and $\Delta N_{Mg} \simeq$ + 0.006) but again positive.

(iv) The model calculations predict that K^+, Sr^{2+} and Mg^{2+} should be "lost" from the aqueous phase due to adsorption onto the fracture material.

(v) The quantity of Na^+ desorbed is balanced by the sum of the quantities of Ca^{2+}, Sr^{2+}, Mg^{2+} and K^+ sorbed on the solid phase. The inverse relationship should be observed in the aqueous phase i.e. the "gains" in Na^+ should be equivalent to the sum of the losses of Ca^{2+}, K^+, Sr^{2+} and Mg^{2+}.

(vi) The model also predicts that the "losses" for the individual ions from the aqueous phase should be in the order $Ca^{2+} \simeq K^+ > Mg^{2+} > Sr^{2+}$.

(vii) It should be noted that it is difficult to justify giving N_B or ΔN_B values to more than two significant figures. However, the calculated values have been deliberatly given to more than two significant places (Table 9) in order to illustrate predicted trends in the behaviour of the cations.

5.3 Estimates of "gains" and "losses" for Na^+, Ca^{2+}, K^+, Mg^{2+} and Sr^{2+} from the aqueous Phase

As briefly discussed in section 3.2.1, the F^- curve is taken to represent the breakthrough curve for a non–sorbing tracer. The breakthrough curves for the individual cations are influenced by exactly the same processes (dispersion etc.) which determine the form of the F^- curve and clearly, if no interactions occur, all curves should be the same. However, the main premise in this work is that the cations do interact with the fracture material, via a cation exchange mechanism, and this interaction will influence the form of their "break–through" curves. It is beyond the scope of this work to model the migration of the cations in the dipole flow field but in previous chapters a cation exchange model was developed which predicted that the aqueous phase should "gain" Na^+ and "lose" Ca^{2+}, K^+, Mg^{2+} and Sr^{2+}. If the F^- curve is normalised to each cation "break–through" curve, then, on the basis of the foregoing argument, any differences in the integrals under the two curves represent a "gain" or a "loss" in the aqueous phase.

Smooth curves for the experimental data ($C^B_{MIX}(t)$), the normalised F^- data ($C^F_{NORM}(t)$) and the difference curves (inserts) are shown for each cation in Figures 10 – 14. The dashed line in each figure represents the concentration of the respective cations in the mixed water at "steady state" (Table 4).

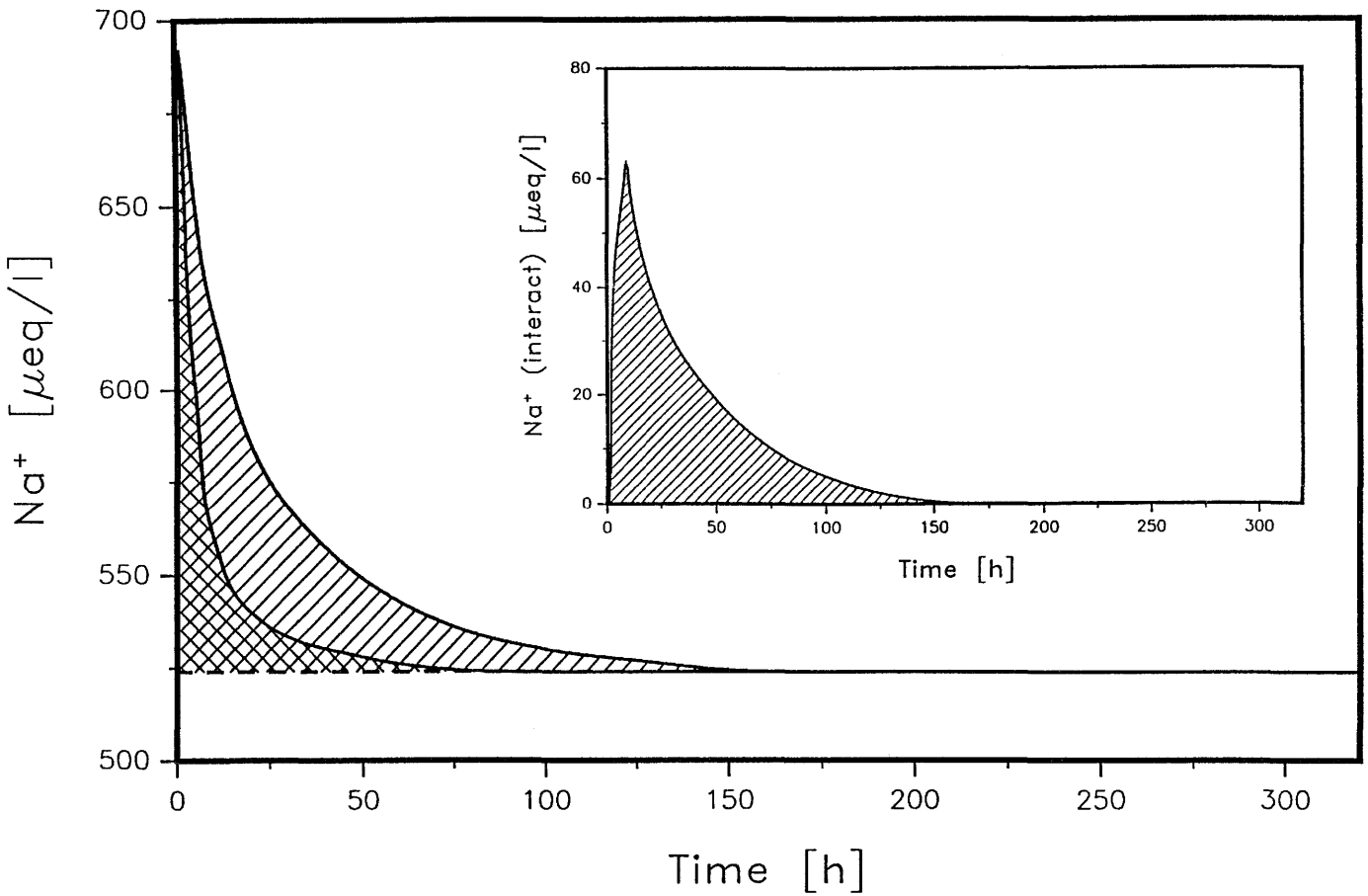

Figure 10: Smooth curves drawn through the measured C^{Na}_{MIX} (upper curve) and normalised C^{F}_{NORM} values as a function of time. The difference between the two curves (hatched region) is shown in the inset figure.

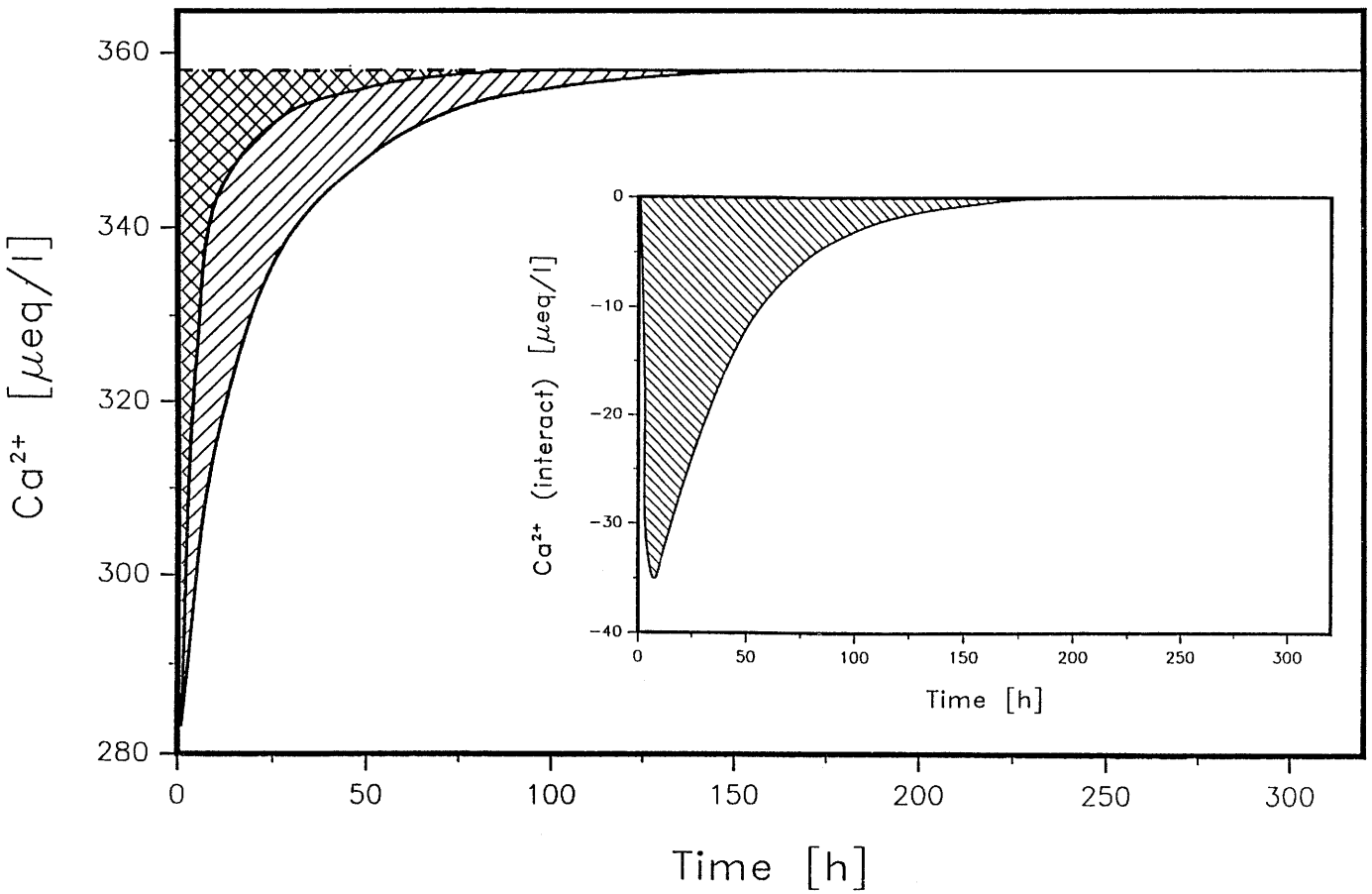

Figure 11: Smooth curves drawn through the measured C^{Ca}_{MIX} (upper curve) and normalised C^{F}_{NORM} values as a function of time. The difference between the two curves (hatched region) is shown in the inset figure.

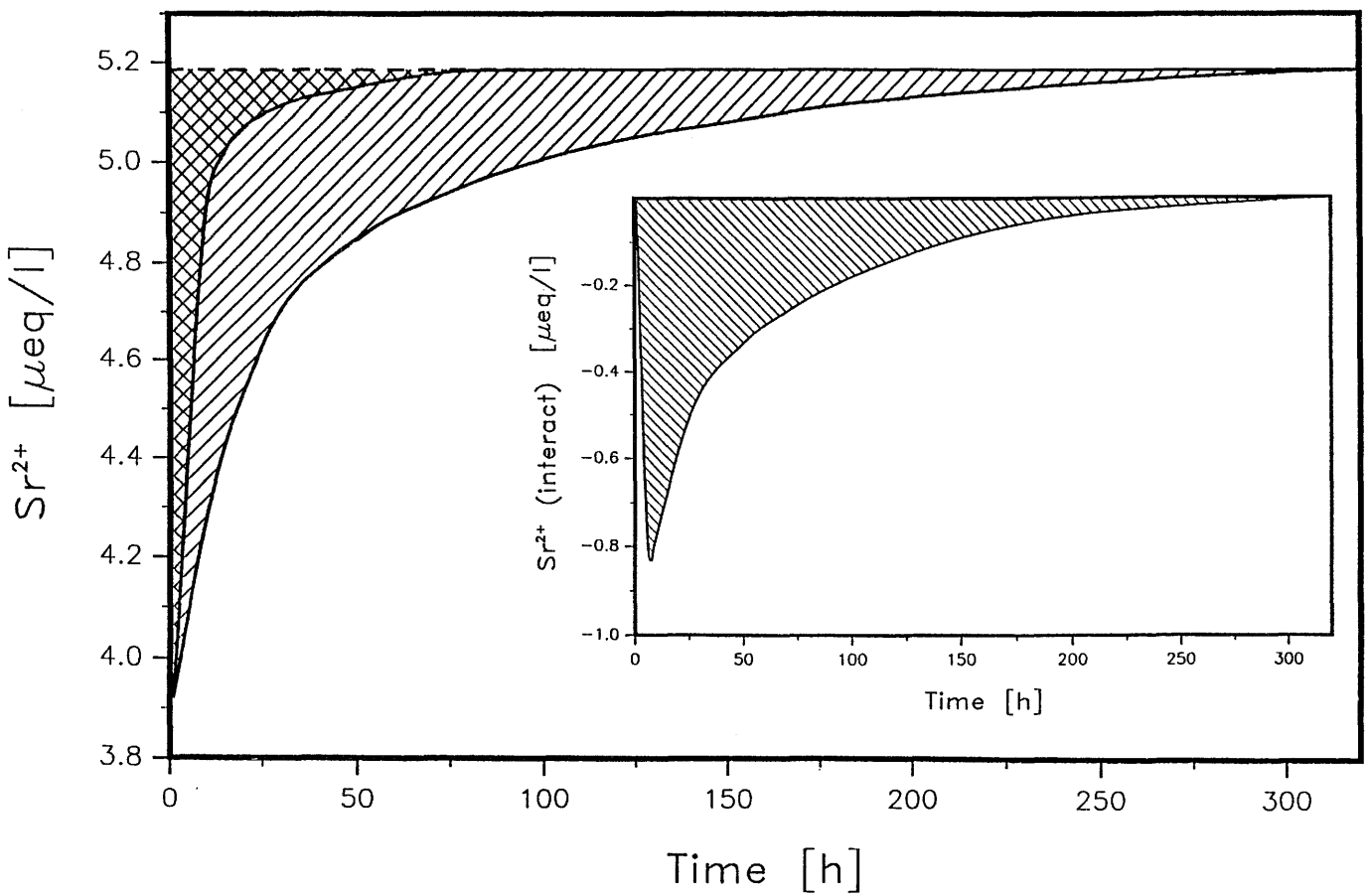

Figure 12: Smooth curves drawn through the measured C^{Sr}_{MIX} (upper curve) and normalised C^{F}_{NORM} values as a function of time. The difference between the two curves (hatched region) is shown in the inset figure.

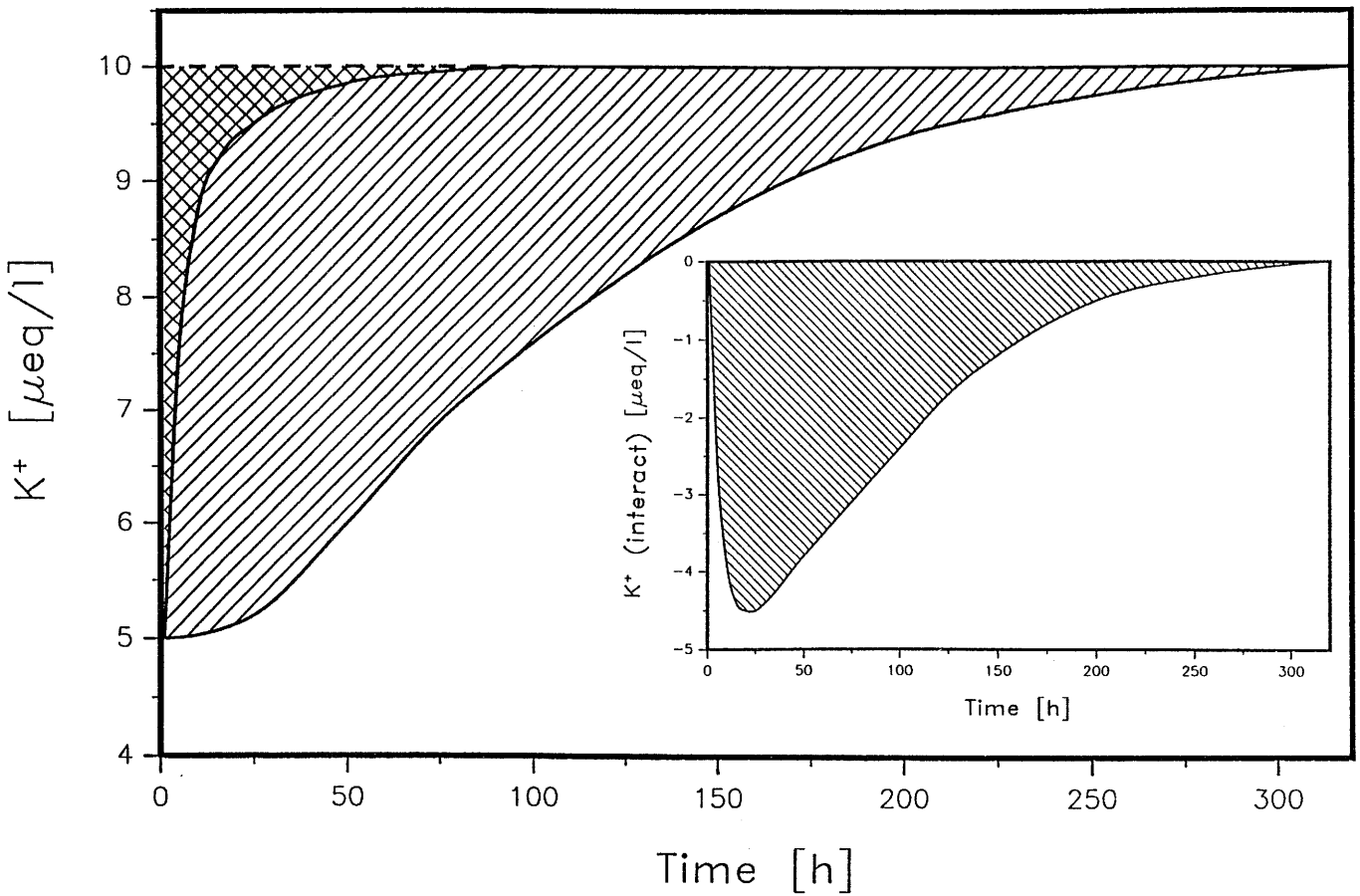

Figure 13: Smooth curves drawn through the measured C^K_{MIX} (upper curve) and normalised C^F_{NORM} values as a function of time. The difference between the two curves (hatched region) is shown in the inset figure.

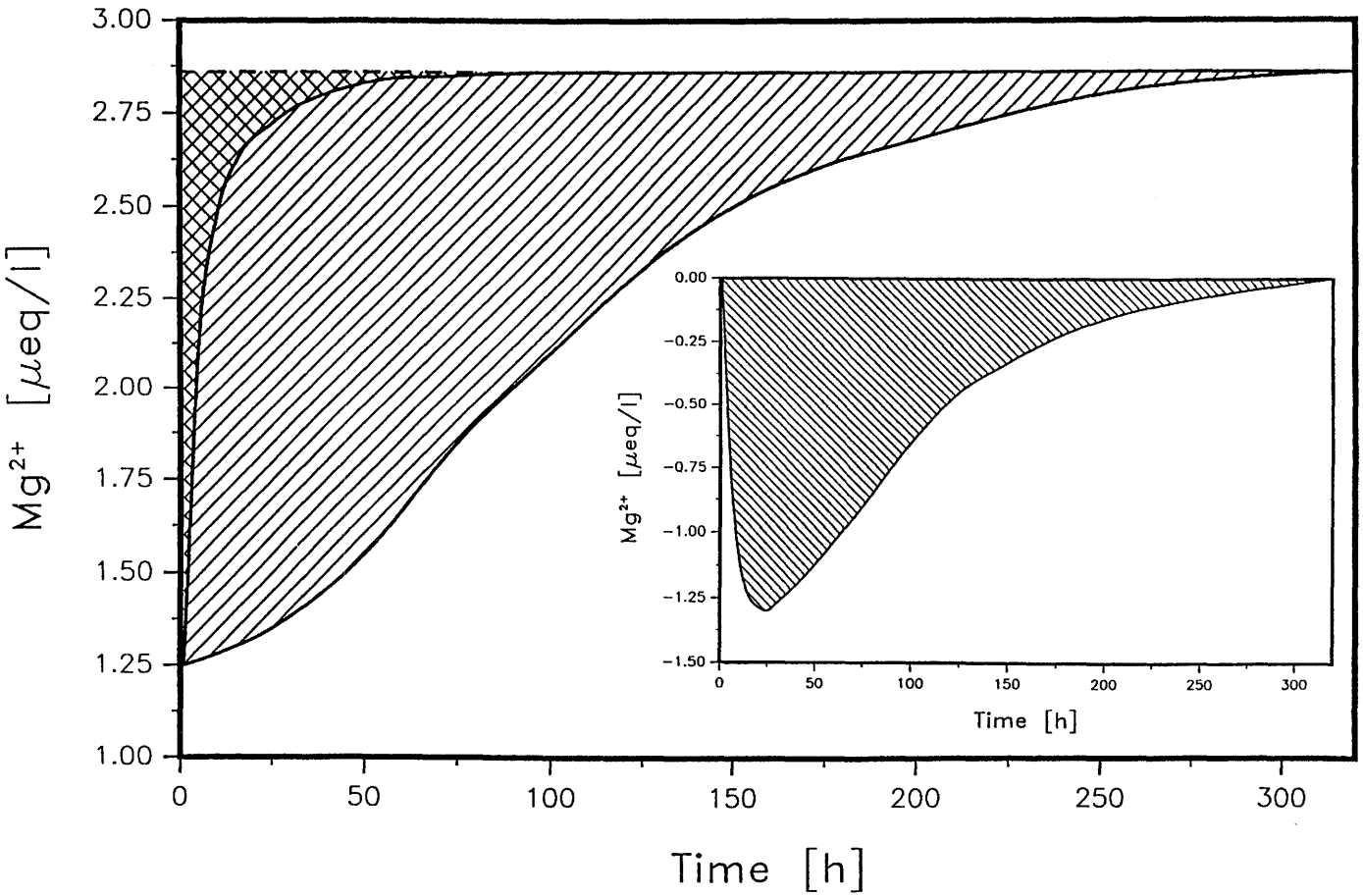

Figure 14: Smooth curves drawn through the measured C^{Mg}_{MIX} (upper curve) and normalised C^{F}_{NORM} values as a function of time. The difference between the two curves (hatched region) is shown in the inset figure.

The difference in the integrated areas (M_B) under the two curves for each cation is given by the following relation:

$$M_B = Q_e \int_0^T C^B_{MIX}(t)dt - Q_e \int_0^T C^F_{NORM}(t) \tag{27}$$

where T is the time to reach steady state conditions ($\sim$ 300 hrs) and Q_e is the extraction water flow rate. M_B–values are given in Table 10 together with the calculated ΔN_B values taken from Table 9. (Areas were determined by graphical integration.) A further quantity, termed the fracture exchange capacity (FEC) and defined as

$$FEC = \frac{M_B}{\Delta N_B} \text{ [meq]} \tag{28}$$

is also included. The FEC is a global number whose magnitude is only valid for the particular dipole flow field in this experiment. In effect it is the product of the mass of fracture material contacted by the flowing water within the dipole flow field and the cation exchange capacity of the fracture.

Table 10: The integrated "gains" (+) and "losses" (–) from the aqueous phase for Na^+, Ca^{2+}, K^+, Mg^{2+} and Sr^{2+} calculated for steady state conditions (t = 300 hrs).

Cation	$M_B^\star$ [meq]	$\Delta N_B^\star$	FEC [meq]
Na^+	+ 15.2 $\pm$ 4.5	-0.040	380 $\pm$ 110
Ca^{2+}	-9.5 $\pm$ 2.9	+0.015	630 $\pm$ 190
K^+	-2.83 $\pm$ 0.4	+0.018	160 $\pm$ 20
Mg^{2+}	-0.92 $\pm$ 0.14	+0.006	150 $\pm$ 20
Sr^{2+}	-0.34 $\pm$ 0.05	+0.001	340 $\pm$ 60

$\star$ The signes are opposite for M_B and ΔN_B since the former refers to the aqueous phase and the latter to the solid phase

From the calculated changes in the ΔN_B values three general deductions were made.

(1) Na^+ is desorbed from the fracture material and Ca^{2+}, Sr^{2+}, Mg^{2+} and K^+ are sorbed.

(2) The absolute magnitude of "gains" or "losses" of these cations on the solid phase is in the order $Na^+ > Ca^{2+} \simeq K^+ > Mg^{2+} > Sr^{2+}$

(3) The quantity "desorbed" from the protomylonite is equal to the quantity "sorbed" onto the fracture material (This must obviously be so for any ion exchange process).

On a qualitative basis, predictions 1 and 2 are in accord with the ΔM_B values given in Table 10. There is a net "gain" of Na^+ in the aqueous phase (desorption from the solid phase) and net "losses" of the other ions. Further, the sum of the "gains" is 15.2 $\pm$ 4.5 meq compared with 13.6 $\pm$ 3.5 meq for the sum of the "losses". These numbers are within 10 % of one another and are therefore in good agreement with the expectation from point (3) and hence with a cation exchange description of the system behaviour. Estimates for the FEC (equation 28) are 380 $\pm$ 110 meq and 340 $\pm$ 90 using M_B values for the sum of "gains" and sum of "losses" respectively and the corresponding ΔN_B values.

The model predictions are, however, less good when M_B and N_B values are looked at in more detail on an individual cation basis. The situation for Na^+ and Sr^{2+} is still good. The FEC values, which should be the same for each pair of M_B and ΔN_B values, are 380 $\pm$ 110 and 340 $\pm$ 60 meq respectively. The agreement here is considered to be acceptable. For the cations K^+, Mg^{2+} and Ca^{2+} the FEC values are 160 $\pm$ 20, 150 $\pm$ 20 and 630 $\pm$ 190 meq, respectively. These values are between a factor of ~ 2 (for K^+ and Mg^{2+}) lower and less than a factor of ~ 2 (for Ca^{2+}) higher than those for Na^+. Such discrepancies can be attributed to various causes. In the cases of $Mg^{2+}$the calculated occupancy changes are exceedingly small and may therefore be very sensitive to the K_c–values used in the equations given in chapter 4. For K^+, even though the selectivity coefficient is a non–linear function of the K^+ occupancy, a constant value was used in the calculations.

Despite the above difficulties, a cation exchange model with the equations and parameters given in chapter 4, appears to be able to provide a good qualitative description of the system behaviour in this experiment and a consistent quantitative description for Na^+. A "best estimate" for the fracture exchange capacity is taken as 360 $\pm$ 100 meq based on the average of the values calculated previously for "gains" in Na^+ and the sum of the "losses" for the other cations.

5.4 Mass of fracture material in the dipole flow field

The FEC is a number which is of little use on its own if the main aim of the foregoing analyses is to attempt to predict/estimate the in situ sorption of Na^+ and Sr^{2+}. However, if this number can be normalised with respect to the mass of fracture material within the volume of the fracture influenced by the dipole flow field, then such a conversion enables the value to be compared with the CEC of mylonite determined in laboratory experiments (Baeyens et al. 1989, Aksoyoglu et al. 1990). In addition, with a known CEC it is possible to estimate K_d values for the Na^+ and Sr^{2+} in the fracture which can again be compared with previous data from rock–water interaction experiments (Baeyens and Bradbury, 1989), with laboratory sorption data (Aksoyoglu et al. 1989), and with the value deduced by Herzog (1990) from an analysis of a migration experiment using ^{24}Na as water tracer.

As a first step in estimating the mass of the fracture material involved in this experiment the volume of water in the fracture within the dipole flow field was estimated from the "break–through" curve for the non–interacting F^- ion, Figure 15. The concentrations given for F^- are those entering borehole 6 from the dipole flow field and were calculated from the experimental data (Table 2) using equation 2. In the figure a smooth curve was drawn through the calculated data points. The dashed line represents the steady state F^- concentration which corresponds to the concentration in the water injected into borehole 4.

With respect to Figure 15, the line PQR was drawn by trial and error such that the cross–hatched regions indicated on either side of this line were of equal area. It follows from this that the areas of the rectangle $C^F_{MI}PRC^F_{inj}$ is equal to the area under the curve $C^F_{MI}Q\ S$ bounded by the lines $C^F_{inj}S$ and $C^F_{MI}C^F_{inj}$ (see insert diagramme).

The volume of water, V_{fw}, contained within the dipole flow field is then given by

$$V_{fw} = t_B Q_i \tag{29}$$

where t_B is the time defined in Figure 15 and Q_i is the injection rate into borehole 4. In order to see that this is so, consider the following mass balance equations in which it is assumed that the injection rate Q_i, into borehole 4, is equal to the flow into borehole 6 from the dipole flow field (see section 4.1).

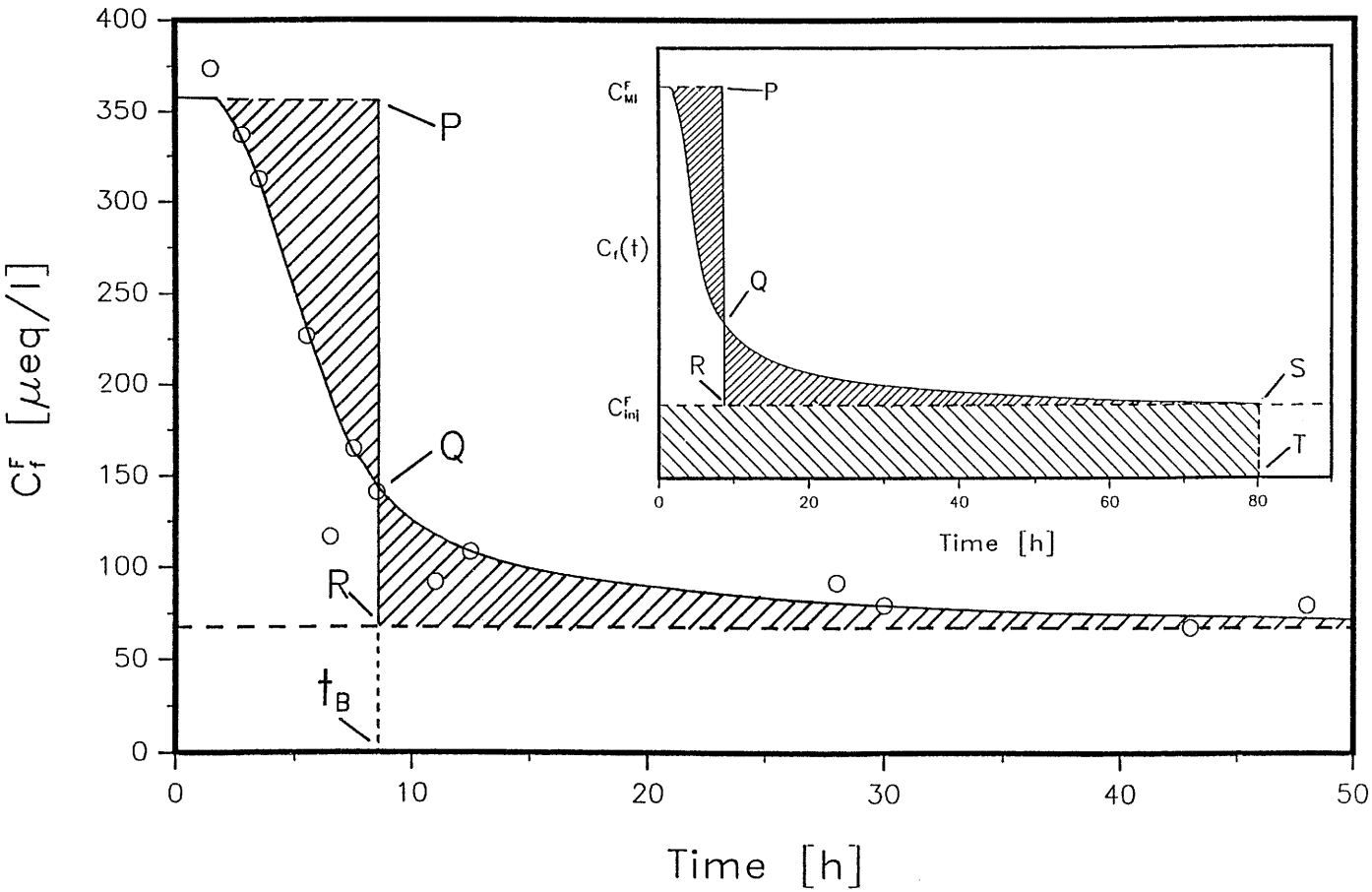

Figure 15: Calculated F^- concentration entering borehole 6 from the dipole flow field.

The mass of F^- initially residing in the volume of the fracture defined by the dipole flow field is:

$$V_{fw}C^F_{MI} \tag{30}$$

where C^F_{MI} is the concentration of F^- in the MI–water. If a steady state is reached after a time, T, the mass of F^- pumped into the system in this time is:

$$TQ_iC^F_{inj} \tag{31}$$

Therefore the total mass of F^- originally in the fracture plus the quantity pumped in is:

$$V_{fw}C^F_{MI} + TQ_iC^F_{inj} \tag{32}$$

At steady state ($t = T$) the concentration of F^- in the water in the dipole flow field has reached a value equal to that of the injected F^- concentration, C^F_{inj}, and the mass is therefore

$$V_{fw}C^F_{inj} \tag{33}$$

The mass of F^- collected in borehole 6 from the dipole flow field is the integral under the curve $C^F_{MI}QS$ between $t = 0$ and $t = T$ i.e.

$$Q_i \int_0^T C^F_F(t)dt \tag{34}$$

Consequently, for mass balance in the system:

$$V_{fw}C^F_{MI} + TQ_iC^F_{inj} = V_{fw}C^F_{inj} + Q_i \int_0^T C^F_F(t)dt \tag{35}$$

or

$$\frac{V_{fw}}{Q_i}(C^F_{MI} - C^F_{inj}) = \int_0^T C^F_F(t)dt - TC^F_{inj} \tag{36}$$

But $\int_0^T C^F_F(t)dt - TC^F_{inj}$ equals the area under the curve $C^F_{MI}QS$ bounded by the lines $C^F_{inj}S$ and $C^F_{MI}C^F_{inj}$ and as shown previously this area is equivalent to the area of the rectangle $C^F_{MI}PRC^F_{inj}$ which is simply $t_B(C^F_{MI} - C^F_{inj})$. Therefore,

$$\frac{V_{fw}}{Q_i}(C^F_{MI} - C^F_{inj}) = t_B(C^F_{MI} - C^F_{inj})$$

hence $V_{fw} = t_BQ_i$, as required. The parameter t_B is calculated to be ~ 9 hours which, with Q_i = 45 ml min^{-1}, gives the volume of water in the fracture volume

within the dipole flow field as 24 litres. If the flow porosity in the fracture is ϵ and the density of the fracture material is ρ then the mass of fracture material, W_f, is given by

$$W_f = V_{fw}\frac{\rho(1-\epsilon)}{\epsilon} \tag{37}$$

The problem with the above equation is that the flow porosity throughout the whole migration fracture cannot be independently determined. However, a recent structural analysis of thin sections taken from cores through the migration fracture (Bossart and Mazurek, 1990) yielded mean flow porosities of 20-30%. In addition, Herzog (1990), in his modelling work on the migration of pulse inputs of non–sorbing tracers (^{82}Br, uranine) and weakly sorbing ^{24}Na, achiefed good quantitative agreement between calculated and experimental breakthrough curves when using a flow porosity of 30 %. This value has been taken here as "a best available estimate". Another reason for choosing the value given by Herzog (1990) is that the calculations of K_d values for ^{24}Na made in the subsequent section will be compared with those derived for Na^+ from the modelling of the migration experiment.

Therefore, putting ϵ = 0.3, ρ = 2.7 x 10^3kg m^{-3} and V_{fw} = 24 x $10^{-3}m^3$ into equation (37) yields a value of 150 kg for the mass of fracture material in the dipole flow field.

5.5 Estimates of the in situ cation exchange capacity of the migration fracture material

The cation exchange capacity of the fracture material in the fracture (CEC_{FRAC}) can be calculated from the experimentally determined fracture exchange capacity, FEC, and the calculated mass of the fracture material, W_f:

$$CEC_{FRAC} = \frac{FEC}{W_f} \qquad [\text{meq kg}^{-1}] \tag{38}$$

Using the data for FEC (section 5.3) and W_f (section 5.4) yields a value of $\sim$ 2.4 meq kg^{-1}. The question then arises as to whether such a value is physically reasonable and meaningful, especially in view of the assumptions which have been made.

The only other independent data which might be considered relevant, and with which

the above estimate might be compared, are the laboratory CEC measurement carried out on a mineralogically similar fracture material obtained from a different fault zone (AU126) intersecting the access tunnel some 30 m distant from the migration fracture. Although it was highly desirable to use material from the migration fracture for the laboratory experiments, this proved to be impractical due to the limited quantities of extractable material, see Bradbury (ed., 1989). These CEC measurements, carried out at a pH of 7, using silver thiourea as the high selectivity complex, ranged in value from $\sim$ 3 meq kg^{-1} ("loosly" disaggregated material and very gentle shaking; in Bradbury (ed., 1989) to $\sim$ 6 meq kg^{-1} (crushed and sieved to < 250 μm) and up to $\sim$ 13 meq kg^{-1} (particles size < 63 μm; Aksoyoglu et al., 1990). A further set of measurements, where the material was disaggregated by vigorous shaking during the CEC determinations, yielded values of $\sim$ 9 meq kg^{-1} (Baeyens, unpublished work). Thus the laboratory CEC data, measured on fracture material from faultzone AU126, are factors of up to 5 times higher than the value calculated from the results of the injection test.

The fracture material from AU126 and from the migration fracture, though in general mineralogically similar, do differ significantly with regard to their contents of muscovite (smectite) and biotite (Meyer et al., 1989) which are important in determining the overall CEC in these materials.

In Table 11, the mineralogy of the two types of fracture material are given together with CEC data for the individual mineral phases (< 63 μm particle size) taken from Allard et al (1983). These data are used to calculate the CEC of the two types of fracture material. As can be seen, the calculated value for the fracture material from AU126 is $\sim$ 14 meq kg^{-1} which compares quite well with the measured value of 13 meq kg^{-1} (< 63 μm particle size). Thus, for a given particle size, estimating the CEC for fracture material in this way seems to be reasonable. What is particularly interesting about the values given in Table 11 is that the CEC for the migration fracture material is approximately a factor of three **lower** than the fracture material from AU126 for which measured data are available. Thus, on the basis of this comparison and the laboratory measurements, the values for the migration fracture material might be expected to lie within the range of $\sim$ 1 to 5 meq kg^{-1}. The CEC value of $\sim$ 2.4 meq kg^{-1} calculated from the results of the EM–water injection experiment lies within the range of values estimated from laboratory data.

Table 11: Calculated CEC values for the fracture material in the migration fracture (AU96) and in fault zone AU126.

MINERALOGY (Particle size < 61 μm)	CEC[a] at pH 8 (meq kg^{-1})	Migration Fracture Protocataclastic Protomylonite Faultzone AU96		Mylonite from Faultzone AU126	
		Fractional content [c]	Contribution to total CEC (meq kg^{-1})	Fractional content [c]	Contribution to total CEC (meq kg^{-1})
Quartz	0.02	0.32	0.06	0.30	0.06
Plagioclase/Albite	0.37	0.32	1.20	0.20	0.74
K–feldspar[b]	0.37	0.19	0.71	0.13	0.48
Chlorite	5	0.01	0.50	–	–
Biotite	1.7	0.09	1.55	0.13	2.21
Muscovite/Sericite	5.2	0.02	1.20	0.21	10.92
Epidote	0.6	0.01	0.08	0.02	0.13
Carbonate	0.02	< 0.01	–	< 0.01	–
Accessories	–	0.02	–	0.08	–
Total calc. CEC	–		5.3		14.5

[a] from KBS 83–64 (Allard et al., 1983)
[b] not included in KBS 83–64 but assumed equal to Albite
[c] from Meyer et al., 1989

5.6 Estimates of in situ K_d values

Upper and lower bounds of $\sim$ 5 and 1 meq kg^{-1}, respectively, were given in the previous section for the in situ CEC of fracture material in the migration fracture. These values can be used together with the fractional occupancy data for fracture material in equilibrium with MI water (Table 9) to estimate in situ distribution coefficients for certain cations using the following relationship

$$K_d^B = \frac{CEC \cdot N_B}{C_B} \quad [\mathrm{m^3 kg^{-1}}] \tag{39}$$

where K_d^B, N_B and C_B are the distribution coefficient, fractional occupancy and con-

centration in the MI–water respectively of cation B. (Cation 'B' is assumed to sorb only by an ion exchange mechanism). The estimated K_d–values for Na^+ and Sr^{2+} are given in Table 12. K_d values between 8.7 x 10^{-5} and 4.4 x 10^{-4} and 3.2 x 10^{-3} and 1.6 x 10^{-2} m^3 kg^{-1} were obtained for Na^+ and Sr^{2+}, respectively.

Table 12: Estimates of in situ K_d–values for Na^+ and Sr^{2+}

Cation	Concentration in MI–water (meq m^{-3}	Ion Occupancy N_B	K_d–values (m^3 kg^{-1}) for MI fracture material		
			CEC lower bound 1 meq kg^{-1}	CEC upper bound 5 meq kg^{-1}	CEC from this work 2.4 meq kg^{-1}
Na^+	6.9 x 10^2	0.060	8.7 x 10^{-5}	4.4 x 10^{-4}	2.1 x 10^{-4}
Sr^{2+}	4.0 x 10^0	0.013	3.2 x 10^{-3}	1.6 x 10^{-2}	7.8 x 10^{-3}

There is only a limited quantity of data available at the moment with which the above estimates can be compared. Herzog (1990) analysed the breakthrough curves of short term pulse inputs of ^{24}Na into the migration fracture at the GTS and deduced a sorption value of $\sim$ 3 x 10^{-4} m^3 kg^{-1} for Na^+. Aksoyoglu et al. (1990) measured, however, distribution ratios of ^{22}Na and ^{85}Sr in the ranges of 2.3 – 3.5 x 10^{-3} and 6.0 – 11.0 x 10^{-2} m^3 kg^{-1}, respectively. These experiments were carried out on crushed mylonite material with particle sizes of < 250 μm and < 63 μm. Their results could be interpreted reasonably well with a cation exchange mechanism. A direct comparison between the estimates for Na and Sr sorption obtained here and the above results are not appropriate because of the different modal compositions of mylonite and protomylonite (migration fracture material) and the significantly different water composition used in the laboratory experiments. However, evidence was presented in section 5.5 which indicated that the CEC of protomylonite is approximately a factor of three less than mylonite. For cations such as Na^+ and Sr^{2+}it is hence expected that their K_d-values will also be a factor of $\sim$ 3 less on protomylonite than on mylonite (see equation 39). Using this correction factor, the sorption of Na^+ and Sr^{2+}on protomylonite might be expected to be in the ranges of $\sim$ 1 x 10^{-3} and $\sim$ 2-3 x 10^{-2} m^3 kg^{-1}. The "best estimates" for the K_d–values for Na^+ and Sr^{2+} applying to the in situ protomylonite fracture material obtained from this work are $K_d(Na) \sim 2 \times 10^{-4}$ m^3 kg^{-1} and $K_d(Sr) \sim 8 \times 10^{-3}$ m^3 kg^{-1}. The field data

are still factors of three to five times lower than the modified values from batch tests since in the latter crushed material was used.

The first field experiments will be carried out with a Na^+ tracer since this is the more weakly sorbing radionuclide. By modelling the break–through curve, the sorption coefficient for Na^+ can be deduced. A useful relationship for the planning of later experiments with Sr can be obtained by using equation 39 to calculate the ratio K_d (Sr)/K_d (Na) i.e.

$$\frac{K_d^{Sr}}{K_d^{Na}} = \frac{N_{Sr}/C_{Sr}}{N_{Na}/C_{Na}}$$

Using the fractional occupancies (N_{Sr} and N_{Na}) given previously and the concentrations of Sr^{2+} and Na^+ in MI–water, this ratio has a value of $\sim$ 40 and is independent of the cation exchange capacity of the fracture material. Therefore with respect to the ratio K_d (Sr)/K_d (Na) it is interesting to compare laboratory and field data. The narrow range of values ($\sim$ 60, rock water interaction experiments, Bradbury and Baeyens, 1989, 30 - 45, batchsorption experiments, Aksoyuglu et al., 1990, $\sim$ 40, this experiment) gives a consistent picture of field and laboratory experiments. Thus, if K_d (Na) is known from the first field tests, the above relationship allows a prediction to be made for K_d (Sr). This will allow predictions to be made for the Sr^{2+} break–through curve prior to beginning the field migration tests.

6 Summary and Conclusions

1. The EM–water injection experiment at the GTS, carried out between borehole BOMI 86.004 (injection) and borehole BOMI 87.006 (extraction) clearly demonstrated that the fracture protomylonite–water system may take many weeks to reach steady state when a "foreign" water is introduced. Therefore EM–water should not be used as a source of injection water in migration tests using sorbing tracers.

2. For the conditions under which this experiment was carried out, the anions reached steady state concentrations in the extracted water within $\sim$ 50 hours, the major cations Ca^{2+} and Na^{+} appeared to require $\sim$ 150 hours, and Sr^{2+} approximately 250 hours. The cations K^{+} and Mg^{2+} probably did not reach steady state at all during the $\sim$ 312 hours duration of the test.

3. In general, two processes are important in determining the concentrations in the extracted water: (i) mixing between the injected "foreign" EM–water and the natural fracture water, MI–water and (ii) interaction between the EM–water with the fracture during the movement from borehole 4 to borehole 6.

4. The anions F^{-} and Cl^{-} were considered to behave as conservative water tracers. This was a reasonable assumption since the breakthrough curves for Cl^{-} and F^{-} were very similar to those of "non sorbing" tracers such as $^{82}Br^{-}$ and Na–fluoresceine from previous tests.

5. Under the assumption that "mixing" and interaction with the fracture were the two main mechanisms determing the extracted water concentration profiles for the cations, and that these processes were linearly additive, cation "interaction" curves were obtained by subtracting the normalised breakthrough curves for F^{-} from the experimental curves for the cations.

6. Integration of the individual cation "interaction" curves indicated that the aqueous phase had "gained" Na^{+} and "lost" Ca^{2+}, K^{+}, Mg^{2+} and Sr^{2+}. Within experimental error, these "gains" and "losses" were charge balanced.

7. The conclusion from the above was that these changes observed in the aqueous phase, were induced by cation exchange reaction between the fracture material and the "foreign" water. In effect, the EM–water injection test was a massive rock–water interaction experiment similar to those conducted previously on a much smaller scale in the laboratory (see Bajo et al. 1989b).

8. The selectivity coefficients for cation exchange reactions, determined from laboratory experiments on mylonite, were applied here to the protomylonite fracture material to calculate the fractional cation occupancies of this material when in equilibrium with MI– and EM–waters.

9. The fractional cation occupancy changes, occurring when the contacting water changed from MI to EM–water were used in conjunction with the integrated

"gains" and "losses" from "interaction" curves to calculate a total fracture cation exchange capacity, FEC. A best estimate for the FEC is given as 360 $\pm$ 100 meq based on average of the calculated "gains" and "losses" of Na^+ and the other cations, respectively as well as on changes in cation occupancies.

10. Estimates of the mass of fracture material in the dipole flow field and total fracture cation exchange capacities, enabled a cation exchange capacity of the fracture material to be calculated. A value of 2.4 meq kg^{-1} was given as the best estimate. The uncertainty in this value could be as high as a factor of 2.

11. The estimated value is somewhat lower than those measured in the laboratory (3 – 13 meq kg^{-1}). The fact that there is a difference should not be too surprising. The fracture material is protomylonite in its natural state, whereas the laboratory measurements were carried out on crushed mylonite samples where the CEC values measured depended strongly on the particle size.

12. The modal mineralogical compositions of mylonite and protomylonite are different. Mineralogical data together with CEC values for individual minerals obtained from the literature were used to calculate the CEC of mylonite and protomylonite. These estimates indicated that the CEC of protomylonite is approximately three times less than mylonite.

13. Under the assumption that cation exchange is the only mechanism contributing to the sorption of Na^+ and Sr^{2+}, estimates of the K_d–values for trace quantities of radioisotopes of these nuclides in the migration fracture were made. The best estimates for Na^+ and Sr^{2+} sorption were $\sim 2 \times 10^{-4}$ and $\sim 8 \times 10^{-3}$ m^3 kg^{-1}, respectively.

14. The ratio of the sorption coefficient of Sr^{2+} to that of Na^+ was calculated to be $\sim$ 40. The relationship used to obtain the ratio was independent of the value of the CEC for the fracture material. This value is close to the ratio calculated from laboratory rock-water interaction experiments ($\sim$ 60, see Bradbury and Baeyens, 1989) and from batch sorption experiments (30–45, see Aksoyoglu et al., 1990). There is thus a good agreement between field and laboratory results, particularly in view of the complexity of the system.

Acknowledgements

We would like to thank R. Alexander, A. Cremers, U. Frick, J. Hadermann, F. Herzog, E. Hoehn and I.G. McKinley for some productive discussions and their critical reviews of this study. We also wish to thank E. Hoehn and T. Fierz for their contributions during the field work at the Grimsel Test Site. R. Keil and M. Gloor are gratefully acknowledged for their analytical work at PSI. The efficiency and patience of Renate Bercher and E. Hochstrasser in typing this manuscript is also gratefully acknowledged.

This work was partially supported by the Swiss National Cooperative for the Storage of Radioactive Wastes, NAGRA.

References

Allard, B., Karlsson, M., Tullbory, E.L. and Larson, S.A. (1983) "Ion exchange capacities and surface areas of some major components and common fracture filling materials of igneous rocks." SKBF–KBS Technical Report 83–64

Aksoyoglu, S., Bajo, C. and Mantovani, M. (1990) "Batch Sorption experiments with I, Br, Sr, Na and Cs on Grimsel mylonite." PSI Bericht Nr.83 and NAGRA Technical Report NTB 91-06

Baeyens, B., Aksoyoglu, S. and Bradbury, M.H. (1989) "Cation exchange characteristics of mylonite."PSI Bericht Nr. 28 and NAGRA NTB 88-23 (Ed. M.H. Bradbury)

Baeyens, B. and Bradbury, M.H. (1989) "Selectivity coefficients and estimates of in–situ sorption values for mylonite." PSI Bericht Nr. 28 and NAGRA NTB 88-23 (ed. M.H. Bradbury)

Bajo, C., Hoehn, E. und Keil, R. (1987) "FLG–MI: Chemische Charakterisierung des Grundwassers am Standort AU 96 m." PSI Internal Report TM–42–87–09

Bajo, C., Hoehn, E., Keil, R. and Baeyens B. (1989a) "Chemical Characterisation of groundwater from the fault zone AU 96 m." PSI Bericht Nr. 28 and NAGRA NTB 88-23 (Ed. M.H. Bradbury)

Bajo, C., Aksoyoglu, S. and Mantovani, M. (1989b) "Groundwater stability and rock–water interaction experiments." PSI Bericht Nr. 28 and NAGRA NTB 88-23 (Ed. M.H. Bradbury)

Bossart, P. and Mazurek, M. (1990) "Strukturgeologische Charakterisierung und Geometrie der Fliesswege in der Migrationsscherzone VT 240, Felslabor Grimsel. Nagra Internal Report NIB 90-44

Bradbury, M.H., ed., (1989), "Laboratory investigations in support of the migration experiments at the Grimsel Test Site." PSI Bericht Nr. 28 and NAGRA NTB 88–23

Bradbury, M.H. and Baeyens, B. (1989) "Application of the results of the GTS Migration experiment." PSI Bericht Nr. 28 and NAGRA NTB 88-23 (ed. M.H. Bradbury)

Bronstein, I.N., Semendjajew, K.A., (1985) "Taschenbuch der Mathematik." 22. Auflage, ed. G. Grosche, V. Ziegeler and D. Ziegler, Verlag Harri Deutsch, Thun und Frankfurt/Main

Eikenberg, J. and Kipfer, R. (1989) "^{4}He als Tracer bei Migrationsversuchen." PSI Internal Report TM–41–89–12

Eikenberg, J. (1989) "Water speciation calculations for the BOEM injection experiment at the GTS." PSI Internal Report TM–41–89–20

Frick, U., Baertschi, P. and Hoehn, E. (1988) "Migration investigations." NAGRA Bull. Spec. Ed. 23 – 34

Frick, U. (ed.) (1990) "Grimsel Test Site Migration Experiment – Synthesis and Status 1990." NAGRA Technical Report NTB 90–14 (in preparation)

Gaines, G.L. and Thomas, H.C. (1953) "Adsorption studies on clay minerals II. A formulation of the thermodynamics of exchange adsorption." J. Chem. Phys. 21, 258–261

Grim, R.E. (1953) "Clay mineralogy." McGraw Hill Book Company, INC. New York–Toronto–London

Hadermann, J., von Gunten, H.R., McCombie, C. and McKinley, I.G. (1988) "Radionuclide Migration in the Geosphere – Swiss research activities in laboratory and field experiments in model validation." Radioactive Waste Management and the Nuclear Fuel Cycle, 10, 233 – 255

Hadermann, J. and Roesel, F. (1985) "Radionuclide chain transport in inhomogenous crystalline rocks, limited matrix diffusion and effective sorption." EIR Report Nr. 551, PSI, Villigen, Switzerland

Herzog, F. (1989) "Modelling the hydrostatic situation at the migration site in the Grimsel Test Site." PSI Bericht Nr. 35 und NAGRA NTB 89–16

Herzog, F. (1990) "A simple transport model for the Grimsel migration experiments." PSI Bericht and NAGRA Technical Report (in preparation)

Hoehn, E., Fierz, T. and Thorne, P. (1989) "Hydrogeological characterisation of the migration experimental area at the Grimsel Test Site." PSI Bericht Nr. 60 and NAGRA NTB 89–15

Jakob, A., Hadermann, J. and Roesel, F. (1989) "Radionuclide chain transport with matrix diffusion and non–linear sorption: RANCHMDNL." PSI Bericht Nr. 54, Würenlingen, NAGRA NTB 90–05, Baden, Switzerland

Lewis, R.C. and Thomas, H.C. (1963) "Adsorption studies on clay minerals, VIII. A consistency test of exchange sorption in the systems sodium–cesium–barium montmorillonite." J. Phys. Chem., 67: 1781 – 1783

McKinley, I.G., Alexander, W.R., Bajo, C., Frick, U., Hadermann, J., Herzog, F.A. and Hoehn, E. (1988) "The radionuclide migration experiment at the Grimsel rock laboratory, Switzerland." Scientific Basis for Nuclear Waste Management XI. 179 – 187.

Meyer, J., Mazurek, M. and Alexander, W.R. (1989) "Petrographic and mineralogical characterisation of fault zones AU 96 and AU 126." PSI Bericht Nr. 28 and NAGRA NTB 88-23 (Ed. M.H. Bradbury)

Thorne, P. (1990) "Grimsel Test Site Migration Experiments: description of borehole, flow control and data acquisition equipement used in the hydrology and pilot tracer test." NAGRA Internal Report NIB 89–12.

Appendix

Estimation of errors

General remarks

If a large number of individual measurements (x_i .... x_n) of the same quantity are available, a mean or probable error can be calculated by application of the Gaussian theory of errors. For this statistical approach a mean value ($\overline{X}$) of the single measurements and the variance (S^2) of the quantity can be calculated according to the following relations:

$$\overline{X} = \frac{1}{n} \sum_{i=1}^{n} x_i \qquad \text{(A1)}$$

$$S^2 = \frac{1}{n-1} \sum_{i=1}^{n} (x_i - \overline{X})^2 \qquad \text{(A2)}$$

The standard deviation (S) yields the absolute error (Δx) of the mean value ($\overline{X}$).

If a quantity F is a function of several variables (F = f (X_i .... X_n)) and each variable has an individual error ΔX_i, then providing that F exhibits continuous partial derivatives of the variables X_i, the error in F, ΔF, can be expressed as (e.g. Bronstein–Semendjajew, 1985):

$$\Delta F \simeq \sum_{i=1}^{n} \left| \frac{\partial F}{\partial X_i} \right| \Delta X_i \qquad \text{(A3)}$$

In the following a brief description is given of the methods used to assign errors to the cation concentrations in the MI, EM–water and the mixed water used in the calculations.

1. **MI–water** (see table 3)

   Unfortunately, no measurements of the MI–water concentration were made prior to starting the MI–water injection experiment. Although, as stated in section 3.2, it is highly likely that the water extracted during the first few hours was "pure" MI water, the number of data points taken during this time were too few to make any reasonalbe estimates of errors. Instead, the approach adopted was to apply the errors calculated for the individual cations in the mixed water at steady state (see point 3) to the MI water.

2. **EM–water** (see table 3)

   The measurements on the single sample of EM water was not usable due to contamination problems. The results of Bajo et al. (1987) were used instead,

being the only data available. The errors given by Bajo et al. (1987) are greater than those calculated for the mixed water since their results include long term temporal variations. Nevertheless, these errors were used in the calculations and hence they are considered, if anything, to overestimate the concentration errors for this water in the experiment.

3. **MI–EM mixed water** (see table 2, measured values)
   The anions reached steady state within $\sim$ 50 hours and most of the cations within $\sim$ 150 hours. Once steady state had been reached, all measurements thereafter should remain constant. Thus the post steady state data were analysed statistically using equations (A1) and (A2) to determine error values. The errors calculated here were assumed to apply to the pre–steady state data also.

4. **Calculated Mixed water compositions, C^B_{MIX}** (see table 4, calculated values)
   Assuming equilibrium,

$$C^B_{MIX} = (1 - X_i)\ C^B_{MI} \ + \ X_i\ C^B_{EM} \qquad \text{(A4)}$$

   The errors in C^B_{EM} and C^B_{MI} have already been discussed. To determine the errors in the calculated C^B_{MIX} values the error in X_i, the mixing parameter, must first be determined. Differentation of equation (1), section 3.3, yields:

$$\Delta X_i \approx \left|\frac{\partial X_i}{\partial Q_e}\right| \Delta Q_e + \left|\frac{\partial X_i}{\partial Q_i}\right| \Delta Q_i \qquad \text{(A5)}$$

   which reduces to

$$\Delta X_i = \left|\frac{1}{Q_e}\right| \Delta Q_i + \left|\frac{Q_i}{Q_e^2}\right| \Delta Q_e \qquad \text{(A6)}$$

   where ΔQ_i and ΔQ_e are equal to $\pm$ 1 ml min^{-1}.
   The error in C^B_{MIX} can then be found from the total differential of equation (A4) i.e.

$$\Delta C^B_{(MIX)} = \left|\frac{\partial C^B_{(MIX)}}{\partial X_{(MI)}}\right| \Delta X_i + \left|\frac{\partial C^B_{(MIX)}}{\partial C^B_{(EM)}}\right| \Delta C^B_{(EM)} + \left|\frac{\partial C^B_{(MIX)}}{\partial C^B_{(MI)}}\right| \Delta C^B_{(MI)} \qquad \text{(A7)}$$

   which yields

$$\Delta C^B_{(MIX)} = (C^B_{(EM)} - C^B_{(MI)})\Delta X_i + X_i \Delta C^B_{(EM)} + (1 - X_i)\Delta C^B_{(MI)} \qquad \text{(A8)}$$

   The relative errors determined for C^B_{MIX} are also displayed in figures 2 – 8.

5. **Integrals of C^B_{MIX}(t)** to obtain M_B–values (see table 10)
   Smooth curves were drawn through the measured data and through the extremes of the error bands. Graphical integration of the three curves then yielded a mean value and an error range.